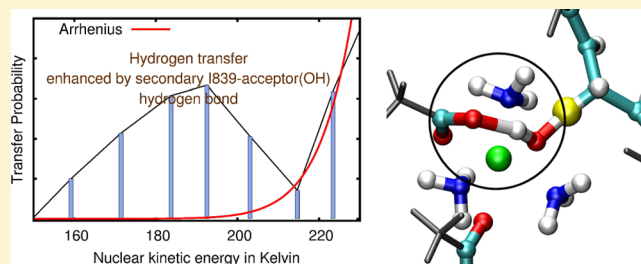


# Active Site Dynamical Effects in the Hydrogen Transfer Rate-limiting Step in the Catalysis of Linoleic Acid by Soybean Lipoxygenase-1 (SLO-1): Primary and Secondary Isotope Contributions

Prasad Phatak, Jordan Venderley,<sup>†</sup> John Debrota,<sup>†</sup> Junjie Li, and Srinivasan S. Iyengar\*

Department of Chemistry and Department of Physics, Indiana University, 800 East Kirkwood Avenue, Bloomington, Indiana 47405, United States

**ABSTRACT:** Using *ab initio* molecular dynamics (AIMD) simulations that facilitate the treatment of rare events, we probe the active site participation in the rate-determining hydrogen transfer step in the catalytic oxidation of linoleic acid by soybean lipoxygenase-1 (SLO-1). The role of two different active site components is probed. (a) On the hydrogen atom acceptor side of the active site, the hydrogen bonding propensity between the acceptor side hydroxyl group, which is bound to the iron cofactor, and the backbone carboxyl group of isoleucine (residue number 839) is studied toward its role in promoting the hydrogen transfer event. Primary and secondary (H/D) isotope effects are also probed and a definite correlation with subtle secondary H/D isotope effects is found. With increasing average nuclear kinetic energy, the increase in transfer probability is enhanced due to the presence of the hydrogen bond between the backbone carbonyl of I839 and the acceptor oxygen. Further increase in average nuclear kinetic energy reduces the strength of this secondary hydrogen bond which leads to a deterioration in hydrogen transfer rates and finally embraces an Arrhenius-like behavior. (b) On the hydrogen atom donor side, the coupling between vibrational modes predominantly localized on the donor-side linoleic acid group and the reactive mode is probed. There appears to be a qualitative difference in the coupling between modes that belong to linoleic acid and the hydrogen transfer mode, for hydrogen and deuterium transfer. For example, the donor side secondary hydrogen atom is much more labile (by nearly a factor of 5) during deuterium transfer as compared to the case for hydrogen transfer. This appears to indicate a greater coupling between the modes belonging to the linoleic acid scaffold and the deuterium transfer mode and also provides a new rationalization for the abnormal (nonclassical) secondary isotope effect results obtained by Knapp, Rickert, and Klinman in *J. Am. Chem. Soc.*, 2002, 124, 3865. To substantiate our findings noted in point a above, we have suggested an I839 → A839 or I839 → V839 mutation. This will modify the bulkiness of hydrogen the bonding residue, allowing greater flexibility in the secondary hydrogen bond formation highlighted above and adversely affecting the reaction rate.



## I. INTRODUCTION

The prevalence of hydrogen transfer reactions<sup>1–3</sup> has been noted in several biological studies.<sup>4–15</sup> The H/D isotope relationship and its effect on the enzyme kinetics has been investigated using experiment and theory for organic as well as enzyme systems.<sup>2,3</sup> Of these studies, the enzyme soybean lipoxygenase-1 (SLO-1) has become a prototype where the hydrogen transfer step is thought to be facilitated, largely, through hydrogen quantum-mechanical tunneling and proton-coupled electron transfer.<sup>16,17</sup> SLO-1 is a nonheme-iron enzyme that catalyzes the oxidation of linoleic acid.<sup>9,18–26</sup> The rate-determining step in the catalytic cycle is the abstraction of a hydrogen atom from the linoleic acid chain by the octahedral Fe<sup>3+</sup>–OH active site complex (see Figure 1). This is followed by a radical attack by O<sub>2</sub> that results in the final peroxide complex.<sup>26</sup> The process displays a large primary kinetic isotope effect ( $k_H/k_D = 81$ ) at room temperature under certain mutations,<sup>27</sup> and also displays a weak temperature dependence of the reaction rate constant.<sup>19,20,27,28</sup>

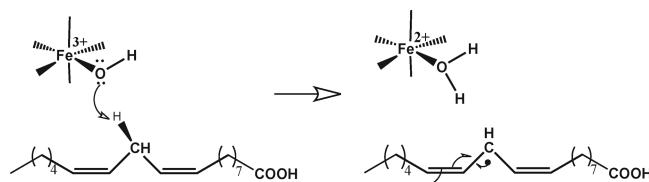


**Figure 1.** Hydrogen abstraction is the rate-determining step in the oxidation of linoleic acid by SLO-1.

There have been several studies on the anomalous primary kinetic isotope effects displayed in SLO-1. For example, Truhlar and co-workers<sup>13,29</sup> have utilized a multidimensional tunneling correction to variational transition state theory,<sup>13,30</sup> where the potential energy surface calculations are obtained using QM/MM techniques.<sup>31</sup> Hammes-Schiffer and co-workers<sup>6,18,17,32,33</sup>

**Received:** March 11, 2015

**Revised:** June 16, 2015

**Published:** June 16, 2015

utilize a vibronically nonadiabatic formalism that includes quantum mechanical contributions from an active electron and an active proton during the proton-coupled electron transfer in SLO-1. Furthermore, Hammes-Schiffer and co-workers have also used similar techniques to study distal mutations in SLO-1<sup>34</sup> and these studies provide a qualitative explanation of the experiments by Klinman and co-workers.<sup>21,35</sup> Warshel and co-workers<sup>9,23,36</sup> have utilized centroid molecular dynamics<sup>37,38</sup> on surfaces computed from empirical valence bond theory.<sup>39–42</sup> Schwartz and co-workers<sup>10</sup> utilize a semiclassical description based on the Langevin equation. A classical dynamics simulation with a Hamiltonian that includes parametrized, analytical potentials and interactions with environment is conducted to find a friction kernel, which is used to calculate the quantum mechanical rate constant using the flux operator formalism.<sup>43</sup> Siebrand and Smedarchina<sup>24</sup> used time-dependent perturbation theory, where the quantum potential is a one-dimensional analytical potential, and finally, Klinman and co-workers<sup>4</sup> compute rates with a vibrationally nonadiabatic methodology<sup>44</sup> that employs Franck–Condon-like overlaps.

In ref 45, one of the authors in this publication investigated the quantum dynamical nature of the hydrogen/deuterium nuclear transfer process in the rate-limiting step of SLO-1. The study explored the quantum effects pertaining to the quantized hydrogen/deuterium nucleus as well as those arising from the electronic degrees of freedom within a reduced active site model system representing SLO-1. The kinetic isotope effect was computed using the transmission amplitude of the wavepacket and the experimental value was reproduced. Some physical insights gleaned from our studies in ref 45 are as follows. (a) Tunneling for both hydrogen and deuterium occurs through the existence of distorted, spherical “s”-type hydrogen nuclear wave functions and “p”-type polarized hydrogen nuclear wave functions for transfer along the donor–acceptor axis. (b) There is also a significant population transfer through distorted “p”-type hydrogen nuclear wave functions directed perpendicular to the donor–acceptor axis [via intervening “π”-type interactions] which underlines the three-dimensional nature of the tunneling process. The quantum dynamical evolution indicates a significant contribution from tunneling processes both along the donor–acceptor axis and along directions perpendicular to the donor–acceptor axis. (c) The hydrogen nuclear wave functions display curve-crossings, in a fashion similar to electronic states. The tunneling process is vibrationally nonadiabatic and is facilitated by these curve-crossings. In ref 45, multiple proton and deuteron excited states (greater than five) were shown to contribute to tunneling. (d) The inclusion of nuclear quantization shifted the transition-state toward the reactants. The precise location of the shifted transition state, however, depends on the populations of each hydrogen and deuterium eigenstate during dynamics.<sup>45</sup> The observations in ref 45 were then reinterpreted using the language of von Neumann measurement theory in ref 46. Several of the qualitative features in ref 45 were reproduced in ref 45 using, in principle, a less strenuous theoretical procedure.

While both refs 45 and 46 utilized reduced models to describe the active site, to facilitate the treatment of the full enzyme using *ab initio* molecular dynamics while keeping in mind the sampling issue of rare events,<sup>48–75</sup> in ref 47, we introduced an approach that (a) retains electronic structural components during nuclear dynamics, (b) combines quantum mechanics/molecular mechanics (QM/MM) treatment,<sup>31,76–96</sup>

as facilitated by the ONIOM procedure,<sup>79,89,95,96</sup> with an asymptotic boundary condition treatment to facilitate the study of the full enzyme,<sup>47</sup> and (c) includes bath variables that guide the nuclear dynamics in the direction of rare events. The approach in ref 47 is suited to treat polarization effects as encountered during processes such as hydrogen transfer reactions and was used to gauge the effect of the flexibility of the active site amino acid groups on the rate determining hydrogen transfer event in the SLO-1 catalyzed oxidation process of linoleic acid. It was found that while the flexibility of the active site indeed had a significant role on the hydrogen transfer event, the backbone carboxylate group attached to an active isoleucine ligand was involved through formation of a secondary hydrogen bond to the acceptor oxygen that accompanied the transfer process. (The particular isoleucine ligand has a residue number 839 in the Brookhaven Protein Data Bank (PDB) structure 1YGE,<sup>97</sup> and is hence referred to as I839 from hereon.) We highlight this hydrogen bond in Figure 2. Using a large number of statistically diverse set of

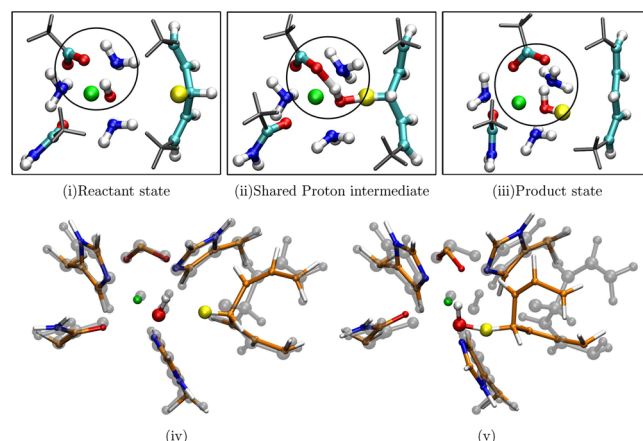


**Figure 2.** Typical snapshots from productive simulations depicting the hydrogen transfer between linoleic acid and the acceptor OH. (i–iii) The depicted system consists of an Fe–OH complex (Fe atom is shown in green), three truncated representations for histidine residues, the backbone carboxylate of the terminal I839 residue, the carboxamide group of Asn694, and a part of linoleic acid substrate that includes the donor carbon ( $C_{11}$ ) group sandwiched between a  $\pi$ -bond on either side. (ii) Stable hydrogen bond network that appears to facilitate the transfer process. When the hydrogen bond formation between I839 and the acceptor group is hindered, the hydrogen transfer process is also adversely affected.<sup>47</sup> (iv, v) Similar behavior displayed in a larger model system.<sup>47</sup>

simulations, we found that the formation of the hydrogen bond was positively correlated to the hydrogen transfer event. A Mulliken charge analysis further reinforced this idea where the electronegativity of the acceptor oxygen was elevated in the presence of the hydrogen bond thereby making it more conducive to accept the transferring hydrogen. In fact, when the active site dynamics was constrained, keeping all other dynamical parameters constant, a monotonic deterioration in the hydrogen transfer probability was noted.

In the current study, we further probe the effect of active site conformational flexibility and specifically the role of the secondary hydrogen bond depicted in Figure 2 on the hydrogen transfer process. We consider primary isotope substitutions, where the hydrogen bonded to the donor carbon atom is deuterated, as well as secondary substitutions where the

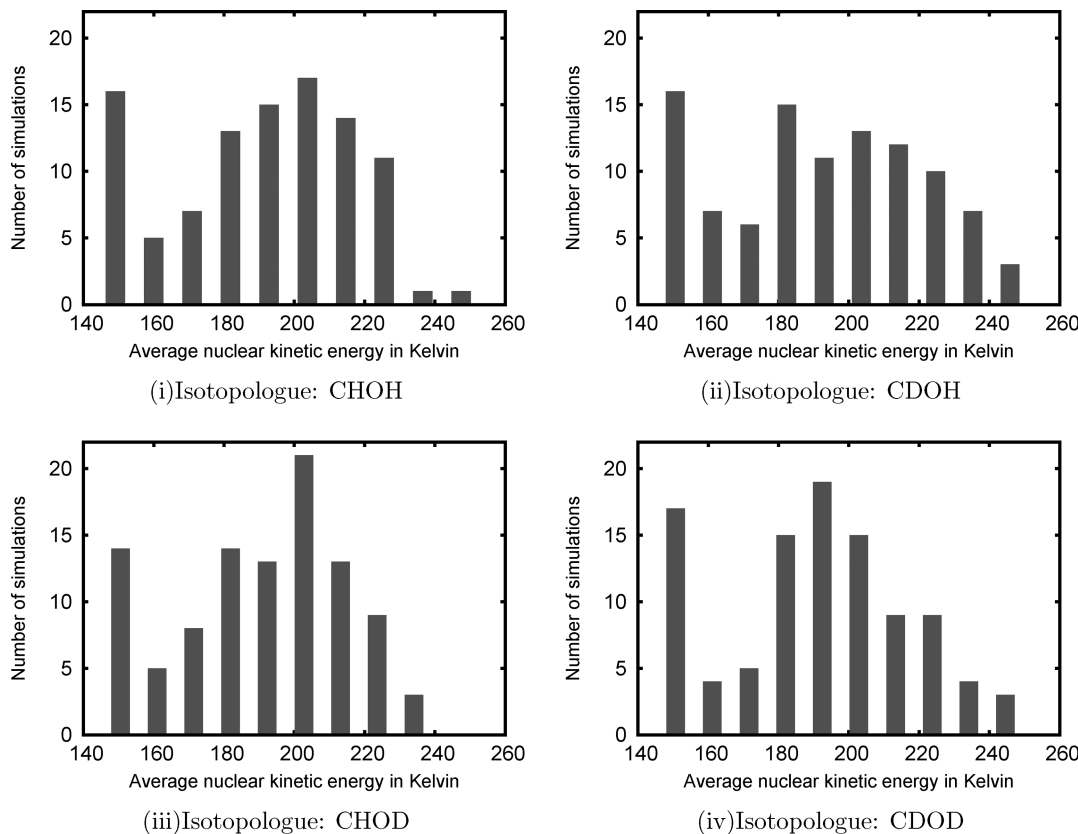


**Figure 3.** Distribution of average kinetic energies in the ensemble of simulations performed. A total of 100 simulations were performed for each isotopically modified system and the kinetic energies presented here are statistical averages obtained from these simulations. The total energy is well conserved in all simulations with RMS deviations of the order of a few tenths of a kcal/mol.

hydrogen atom bound to the acceptor oxygen is replaced by its deuterated counterpart. To inspect secondary effects arising from the donor-side, linoleic acid scaffold, we consider a vibrational analysis which allows us to compute the vibrational coupling involved during the process of a productive (prone to hydrogen transfer) dynamics trajectory. We thus consider four different isotopologues of the SLO-1 active site that are represented using the nomenclature CHO<sub>H</sub>, CHOD, CDO<sub>H</sub>, and CDOD where CX refers to the donor C<sub>11</sub>-H/D group and OX refers to the acceptor O-H/D group. We construct a large number of atom-centered density matrix propagation trajectories (ADMP)<sup>47</sup> that sample rare events for these systems. The rationale behind our choice to probe these secondary hydrogen bonds arises from previous studies<sup>98</sup> where deuterium substitutions in hydrogen bonded systems leads to large variations in the manner in which vibrational modes couple and energy gets redistributed. These greatly affect the temperature dependence<sup>98</sup> of energy transfer. As noted above, there have been several efforts to quantitatively describe the anomalous primary isotope effect in SLO-1. But theoretical studies that probe how secondary isotopic variations modify the transfer process have been limited. In fact, to the best of our knowledge, this is the first such attempt. At the end, by probing the microscopic role of the donor side and acceptor side groups, we are in a position to suggest experimental mutations that could gauge this effect.

This paper is organized as follows: The rare events sampling methodology is summarized in Appendix A since it is already presented in detail in ref 47. To probe the isotope dependent dynamical interplay between the various active site vibrational

degrees of freedom and the hydrogen transfer event, we employ the techniques discussed in section II. In section III, we present the results that are also supported in part through Appendix B. Conclusions are given in section IV.

## II. METHODS TO QUANTITATIVELY GAUGE THE EFFECT OF ACTIVE SITE VIBRATIONS ON REACTIVE EVENTS

The isotopically modified systems are modeled using the algorithms presented in the Appendix A, with more details given in ref 47. The computations are performed for a range of temperatures as shown in Figure 3, with details on the simulation protocols provided in section IIIA. Results of these simulations along with a comparison of H/D transfer probabilities are discussed in Section IIIB. In the current section, we discuss computational strategies to gauge the effect of active site dynamical fluctuations on the H/D transfer event and these techniques are used in sections IIIC and IIID to analyze the results presented in section IIIB.

Specifically, here, we present techniques to probe: (a) the role of active site molecular vibrations and the mechanism by which these couple to facilitate H/D transfer, (b) the isotope dependence of such coupling, and (c) common vibrational characteristics between multiple productive trajectories. The methods discussed in this section are closely related to the approaches in refs 98–101 and are motivated by the idea of energy redistribution in chemical systems.<sup>102–114</sup>

The *ab initio* dynamics trajectories employed here provide the nuclear positions and nuclear velocities:  $\mathbf{R}(t)$ ,  $\mathbf{V}(t)$ , and the electronic density matrix and density matrix velocity:  $\mathbf{P}(t)$  and

$\mathbf{W}(t)$ , as a function of time. The finite-time Fourier transforms for the simulation averaged mass-weighted nuclear velocities for the  $i$ th atom and the  $j$ th degree of freedom,

$$\tilde{\mathbf{V}}_{i,j}(t) \equiv \left( \frac{\sqrt{M_i}}{T} \right) \mathbf{v}_{i,j}(t) \quad (1)$$

are

$$\nu_{i,j}(\omega) = \int_{t=0}^{t=T} dt \{ \exp(-i\omega t) \tilde{\mathbf{V}}_{i,j}(t) \} \quad (2)$$

where  $T$  is the length of simulation. The expression above defines the frequency space oscillations that appear during dynamics, and the quantity

$$\mathcal{F}_v(\omega) = |\nu(\omega)|^2 \equiv \sum_{i,j} |\nu_{i,j}(\omega)|^2 \quad (3)$$

is proportional to the average kinetic energy of the system at frequency  $\omega$  during dynamics. [This result follows from Parseval's theorem,<sup>115</sup> in the limit  $T \rightarrow \infty$ .] By computing  $\mathcal{F}_v(\omega)$ , we probe the differences between the spectral representations for productive and nonproductive events. As we note in the results section, there exists frequency ranges where the behavior of  $\mathcal{F}_v(\omega)$  is significantly different for reactive events that lead to a H/D transfer and those that do not. To probe the nature of molecular modes that contribute to these differences, we provide two approaches that are described in the subsections below.

**A. Decomposing  $\nu(\omega)$  (Eq 2) in Terms of Characteristic Modes to Gauge Energy Redistribution during Reactive Trajectories.** We first project the Fourier transform of the mass-weighted velocities,  $\nu(\omega)$ , onto a complete set of harmonic normal mode vectors,  $\{\vec{H}_i^R\}$ , that are obtained through diagonalization of an electronic Hessian matrix. The superscript "R" corresponds to a chosen nuclear geometry where the Hessian is computed. In this publication, the reactant geometry is used as reference. [This choice provides a convenient language for our discussion, and does not in any way affect the final conclusions in accordance with the completeness relation that exists for the eigenvectors of the Hessian matrix.] The contribution from  $\vec{H}_i^R$  at a specific frequency,  $\omega$  is given by

$$C_i(\omega) = \vec{H}_i^R \cdot \nu(\omega) \quad (4)$$

which is obtained by considering  $\nu(\omega)$  as a linear combination of  $\{\vec{H}_i^R\}$ :

$$\nu(\omega) = \sum_i C_i(\omega) \vec{H}_i^R \quad (5)$$

At the beginning of the dynamics (at time,  $t = 0$ ), a set of modes are populated according to

$$\vec{\mathbf{V}}(t=0) = \sum_i \tilde{C}_i(t=0) \vec{H}_i^R \quad (6)$$

As the dynamics evolves, the harmonic approximation breaks down and the system begins to sample diverse regions of phase-space. The resultant modes can be represented using a coupled set of Harmonic modes and the associated time-dependence may be given by

$$\vec{\mathbf{V}}(t) = \sum_i \tilde{C}_i(t) \vec{H}_i^R \quad (7)$$

where

$$\tilde{C}_i(t) = \vec{H}_i^R \cdot \vec{\mathbf{V}}(t) \quad (8)$$

The components of the vector  $\vec{\mathbf{V}}$  are defined in eq 1. Using eq 2, we note that  $C_i(\omega)$  is the Fourier transform of  $\tilde{C}_i(t)$ . While  $\tilde{C}_i(t)$  represents the time-dependent redistribution of energy as depicted in the reference frame of  $\{\vec{H}_i^R\}$ ,  $C_i(\omega)$  captures the cumulative effect of the  $i$ th mode on the trajectory as manifested at frequency,  $\omega$ . It must further be emphasized that the physics of the problem contained in  $\{\tilde{C}_i(t)\}$  is independent of the choice of basis given the completeness of these basis vectors. Furthermore, the contribution from mode  $i$  within a spectral window,  $[\omega_1, \omega_2]$  is given by

$$C_i^{[\omega_1, \omega_2]} = \left[ \int d\omega G^{[\omega_1, \omega_2]}(\omega) |C_i(\omega)|^2 \right]^{1/2} \quad (9)$$

where  $G^{[\omega_1, \omega_2]}(\omega)$  is a smooth function with nonzero contributions inside  $[\omega_1, \omega_2]$  and zero otherwise. Here  $G^{[\omega_1, \omega_2]}(\omega)$  is chosen to be a normalized skew-Gaussian function, defined as the product of the error function and a Gaussian function, localized within the chosen spectral window,  $[\omega_1, \omega_2]$ . The absolute value squared of the quantity in eq 9, i.e.  $|C_i^{[\omega_1, \omega_2]}|^2$ , is the energy of the system along the  $i$ th mode within the frequency window  $[\omega_1, \omega_2]$ , provided the window function,  $G^{[\omega_1, \omega_2]}(\omega)$ , is appropriately normalized. In this publication, eq 9 is used to analyze the differences in spectral contributions between productive and nonproductive simulations.

**B. "Effective" Modes That Participate in the H/D Transfer Process.** To probe the commonalities between multiple trajectories that display an H/D transfer event, all of which have features inside the frequency window  $[\omega_1, \omega_2]$  (see the results sections), we first define the vector  $\nu_g^{[\omega_1, \omega_2]}$  as

$$\nu_g^{[\omega_1, \omega_2]} = [\int d\omega G^{[\omega_1, \omega_2]}(\omega) |\nu(\omega)|^2]^{1/2} \quad (10)$$

As in the case of  $|C_i^{[\omega_1, \omega_2]}|^2$ , the quantity  $|\nu_g^{[\omega_1, \omega_2]}|^2$  is proportional to the kinetic energy of the system in  $[\omega_1, \omega_2]$ . As seen in the results section of the paper, there exists critical differences in the values for  $\nu_g^{[\omega_1, \omega_2]}$  in certain frequency ranges between simulations that contain a reactive event and those that do not. As a result, the vector in eq 10 is computed for all productive simulations and assembled as columns to form a matrix depicted as  $\Upsilon$ . The number of columns in  $\Upsilon$  is the number of productive simulations and the number of rows is  $3N$ , for  $N$  atoms. A singular value decomposition (SVD)<sup>115–117</sup> of  $\Upsilon$ :

$$\Upsilon = \mathbf{U} \Sigma \mathbf{V}^T \quad (11)$$

leads to composite modes that are common among the productive trajectories and contribute to the window  $[\omega_1, \omega_2]$ . Specifically, here  $\mathbf{U}$  and  $\mathbf{V}^T$  are biorthogonal matrices<sup>116</sup> and  $\Sigma$  is a diagonal singular value matrix. The columns of  $\mathbf{U}$  are the composite modes whereas the columns of  $\mathbf{V}$ , in conjunction with the singular values in  $\Sigma$  represent the extent to which a given singular value, singular vector pair contributes to  $\Upsilon$ . For example,

$$\Upsilon_{i,j} \approx \sum_{k=1}^{N_{SVD}} \mathbf{U}_{i,k} \Sigma_{k,k} \mathbf{V}_{j,k} \quad (12)$$

where  $N_{SVD}$  is the number of significant singular values.

In the results section,  $\nu_g^{[\omega_1, \omega_2]}$ ,  $C_i^{[\omega_1, \omega_2]}$  and the singular vectors of  $\Upsilon$  are used to compare reactive and nonreactive events. The singular vectors of  $\Upsilon$  yield composite modes that are common between productive trajectories and provide insights into participation from specific active site atoms such as secondary hydrogen atoms on the donor and acceptor side. The quantities  $\nu_g^{[\omega_1, \omega_2]}$  and  $C_i^{[\omega_1, \omega_2]}$  provide measures to characterize the differences between reactive and nonreactive events.

### III. PROBING THE ISOTOPE-DEPENDENT HYDROGEN TRANSFER EVENT IN SOYBEAN LIPOXYGENASE-1 (SLO-1) USING THE RARE EVENTS SIMULATION DATA

The isotopically modified systems are modeled using the algorithms in the appendices. A large number of simulations (100 simulations for each isotopologue resulting in a total set of 400 simulations) are performed. These simulations survey a range of internal kinetic energies as depicted in Figure 3. As a consequence, we expect that a wide range of conformational degrees of freedom, and active site conformations, are sampled during these calculations. We use a model system similar to that in ref 45 and construct dynamical trajectories using the methodology in ref 47 that is also briefly outlined in Appendix A. Simulation details are given in Section IIIA. We then analyze the trajectories using ideas in Section II.

**A. Simulation Details.** In ref 45, we employed a reduced active site model<sup>45,46</sup> to investigate the computationally demanding quantum dynamical properties<sup>45</sup> of the transferring proton along with concerted changes in electronic structure. Following this, in ref 47, we used a similar reduced active site model to investigate the role of conformational flexibility and electronic dependence on the hydrogen transfer process in SLO-1. Specifically, ref 47 investigated the role of active site truncation through comparisons with full enzyme simulations modeled using a QM/MM generalization of the rare-event ADMP protocol. Since the agreement between these simulations was reasonably good, in the current study, we employ a truncated active site model, similar to that in refs 45–47, to gauge the effect of isotope substitution on the rate-limiting hydrogen transfer step in SLO-1. The model system consists of a reduced active site comprising 50 atoms. (Figure 4) The electronic energy and gradients during dynamics are computed using ONIOM<sup>79,94,95</sup> with DFT(B3LYP/LANL2DZ) on the higher level and Dreiding<sup>118,119</sup> treatment at the lower level. (See eq A2.) Trajectories are computed using the AIMD rare events simulations method discussed in the previous section. The QM system consists of 34 atoms that include Fe–OH complex, three histidine residues each modeled as ammonia, the backbone carboxylate of the terminal I839 residue, the carboxamide group of Asn694, and a part of linoleic acid substrate that includes the donor carbon ( $C_{11}$ ) group sandwiched between a  $\pi$ -bond on either side.

For the ADMP rare-events sampling dynamics, the fictitious inertia-tensor scale value was chosen to be 0.1 amu·bohr<sup>2</sup> ( $\approx 180$  au) as in previous studies<sup>47,95,120</sup> along with a time-step of 0.25 fs. The donor (carbon), acceptor (oxygen), and the transferring particle (hydrogen or deuterium) are tethered to bath particles with the constraint  $\eta$  chosen to be harmonic (eq

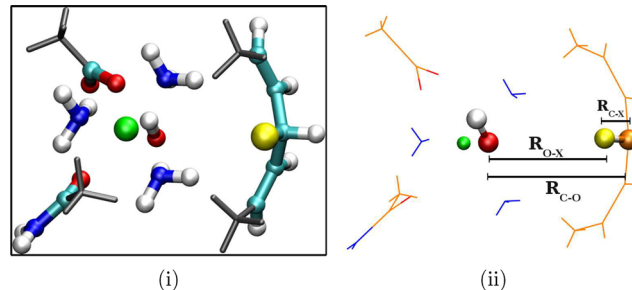


**Figure 4.** (i) Reduced active site SLO-1 model system of 50 atoms used for the AIMD simulations. The system consists of the Fe–OH complex, three histidine residues each modeled as ammonia, the backbone carboxylate of the terminal I839 residue, the carboxamide group of Asn694, and a part of linoleic acid substrate that includes the donor carbon ( $C_{11}$ ) group sandwiched between a  $\pi$ -bond on either side. (b) In this study, the two displayed protons, the primary transferring proton shown in yellow, and the secondary proton that is involved in the hydrogen bond presented in Figure 2, shown in white, are replaced with heavier (deuterium) isotopes. As a result there are four separate systems considered here and these are represented as follows. The system CHOH depicts the original, unsubstituted SLO-1 active site whereas CDOH implies the system where the transferring proton is deuterated. Similarly, CHOD represents the case where the secondary location is deuterated and CDOD is one where both atoms are deuterated. In addition, the reaction coordinate,  $R_c$  (transferring H or D represented as X) is also defined here as  $R_c = (R_{c-X} - R_{O-X}) / R_{c-O}$ .

A3) with force constant of 15570 pN/Å as benchmarked in ref 47. The masses for the bath particles tethered to the donor and acceptor are 500 amu, and that for the transferring particle have a mass of 100 amu. These parameters are consistent with those from previous studies.<sup>47</sup> The computations are performed for a range of temperatures as shown in Figure 3.

**B. Isotope-Dependent Correlated Reactive Events.** To gauge reactivity for each simulation, we monitor the hydrogen transfer process through evolution of the reaction coordinate defined as,

$$R_c = (R_{c-X} - R_{O-X}) / R_{c-O} \quad (13)$$

where the quantity  $R_c$  is a function of simulation time and atoms C, O, and X refer to the donor carbon ( $C_{11}$ ), acceptor oxygen (O) and transferring H or D atom, respectively. (See Figure 4(ii) for a definition.) The evolution of  $R_c$  for a representative set of trajectories is shown in Figure 5. As may be noted, the probability of H/D transfer does not appear to monotonically increase with increase in average nuclear kinetic energy. For example, some of the higher nuclear kinetic energies (shown in red) yield poorer transfer probabilities as is seen from the smaller values of  $R_c$  for larger simulation times. Further analysis of  $R_c$  for the full population of trajectories in Figure 6 indicates the fraction of reactive trajectories as a function of internal kinetic energy (presented in units of kelvin). Finally, Figure 7 indicates a definite correlation between trajectories that include a hydrogen transfer event and those containing the formation of a stronger secondary hydrogen bond between the acceptor oxygen and I839. In all cases the I839-oxygen acceptor oxygen donor–acceptor distance is approximately 0.30–0.37 Å shorter for simulations where there is a hydrogen transfer event. In fact, this difference is smaller when the primary hydrogen is deuterated (0.298 and 0.336 Å) as compared to when the primary hydrogen is a protium (0.362 and 0.367 Å). This indicates an isotope

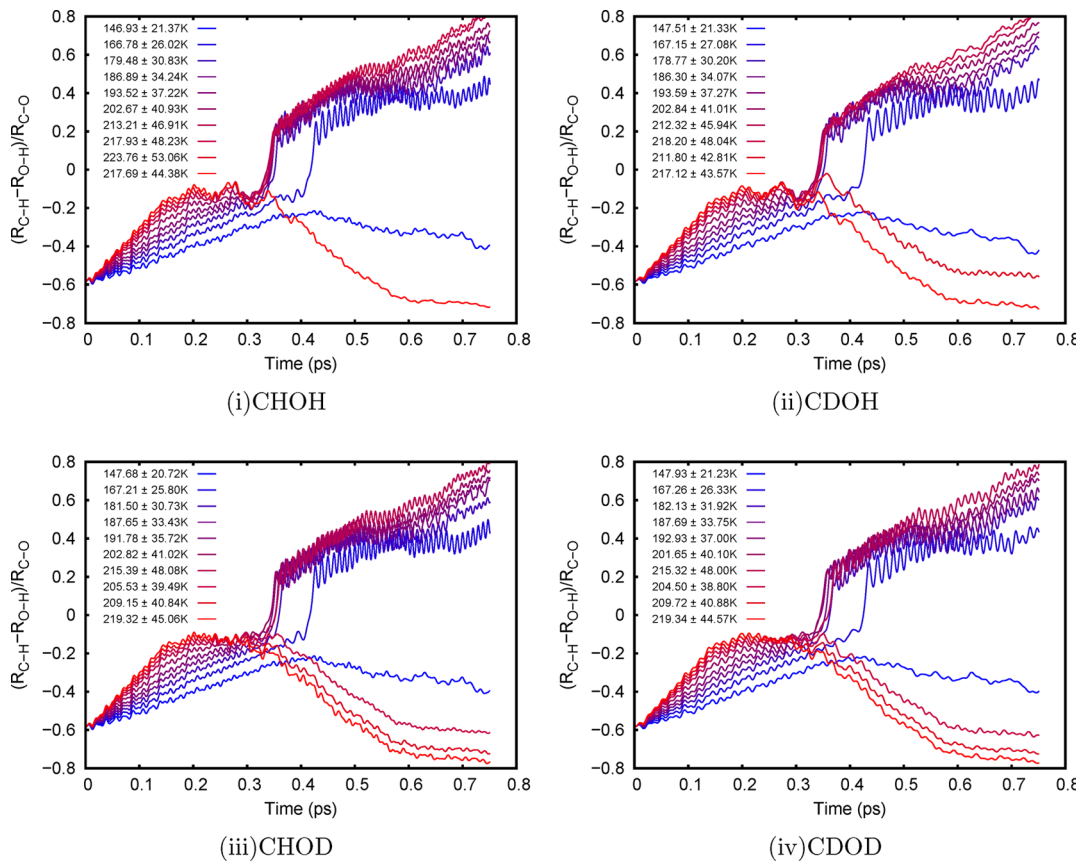


**Figure 5.** Evolution of the reaction coordinate,  $R_\sigma$ , for (a) CHOH, (b) CDOH, (c) CHOD, and (d) CDOD. The quantity,  $R_\sigma$ , along with the system nomenclatures are described in the caption for Figure 4. The plots indicate that the hydrogen transfer probability does not monotonically increase with increasing internal kinetic energy. This is further substantiated in Figure 6 where the full range of simulations is considered.

dependent correlation between the I839-oxygen acceptor oxygen hydrogen bond and a hydrogen transfer event.

Associated with this correlated effect, we find an interesting average nuclear kinetic energy dependent behavior in Figure 6. For all cases, initially, as the average nuclear kinetic energy within the active site model increases, reaction probability increases. But beyond a certain point, increase in kinetic energy, destabilizes the formation of the secondary I839-oxygen acceptor hydrogen bond and reduces reactivity. As the average nuclear kinetic energy is increased even further, the energy deposited into the transfer mode increases and the reactivity starts increasing again. This explains the nonmonotonic (zigzag) nature of the dependence depicted in Figure 6. The second part of this cycle, alludes to the importance of the secondary hydrogen bond. Furthermore, the crossover point occurs at different values of average nuclear kinetic energy for different isotope substitutions. For example, when the secondary hydrogen is a protium, the turnover occurs at a higher value as compared to when the secondary hydrogen is a deuterium. It is also important to note here that the nonmonotonic behavior seen in Figure 6 is not due to a sampling issue; in fact, the relevant range is well-sampled as noted from Figure 3.

To substantiate our findings, we suggest an I839 → A839 or I839 → V839 mutation. This will modify the bulkiness of I839, allowing greater flexibility in the secondary hydrogen bond formation highlighted above and adversely affecting the reaction rate.

**C. Analysis of  $C_i^{[\omega_1, \omega_2]}$  in Eq 9.** In the previous section we have shown how the secondary hydrogen bond between the acceptor oxygen and I839 participates in the H/D transfer event. This appears to explain the anomalous, nonmonotonic, behavior seen in Figure 6. Here, and in the next section, we further gauge this cooperative behavior; we inspect the critical vibrational modes that differentiate productive from non-productive trajectories.

Toward this, we first compute the velocity autocorrelation function in eq A3, which is proportional to the average kinetic energy of the system at frequency  $\omega$ . We then project its components ( $\nu_{ij}(\omega)$  in eq 2) onto a complete basis of harmonic modes (eq 4), that are calculated from the Hessian at the reactant geometry. We find that for all four isotopic systems (CHOH, CDOH, CHOD, and CDOD),  $\mathcal{F}_v(\omega)$  is distinctly different in the  $\sim 3900\text{--}4600\text{ cm}^{-1}$  region for CHOX systems and  $\sim 2800\text{--}3500\text{ cm}^{-1}$  region for CDOX systems. Note that these frequency windows are related by the simple, reduced mass related, scaling factor of  $\sqrt{2}$ . By analyzing the corresponding  $C_i(\omega)$  values (eq 4) from all modes, we find that the donor  $C_{11}\text{--}X$  stretch mode contributions are distinctly different between the productive and nonproductive simulations in the above-mentioned frequency window. An example of this behavior is shown in Figure 8, where the distinguishable spectral window is highlighted. (The harmonic modes used in each case to facilitate this factorization are presented in Figure 11 in Appendix B.) For the CHOX isotope systems, a distinct broad feature is present in the  $\sim 3900\text{--}4600\text{ cm}^{-1}$  region (highlighted by a band in Figure 8, parts i and ii), for some

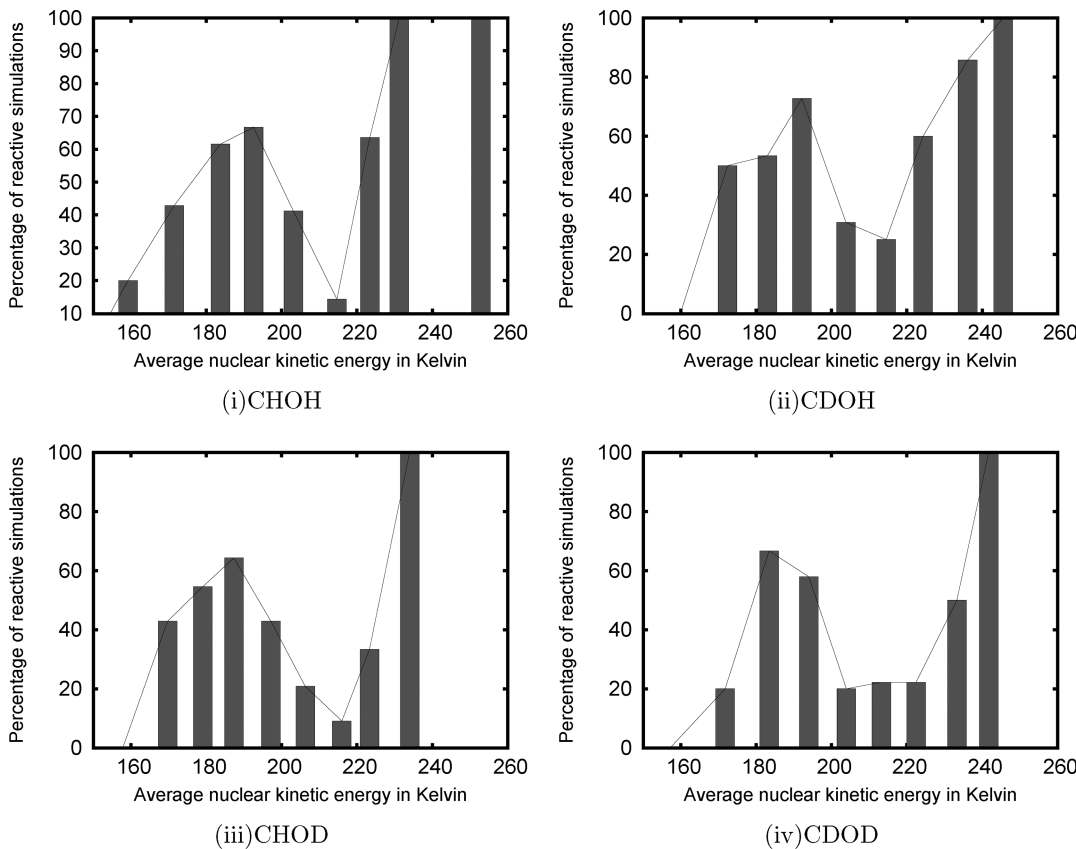


**Figure 6.** Distribution of productive simulations for the full ensemble of calculations. Also see Figure 3

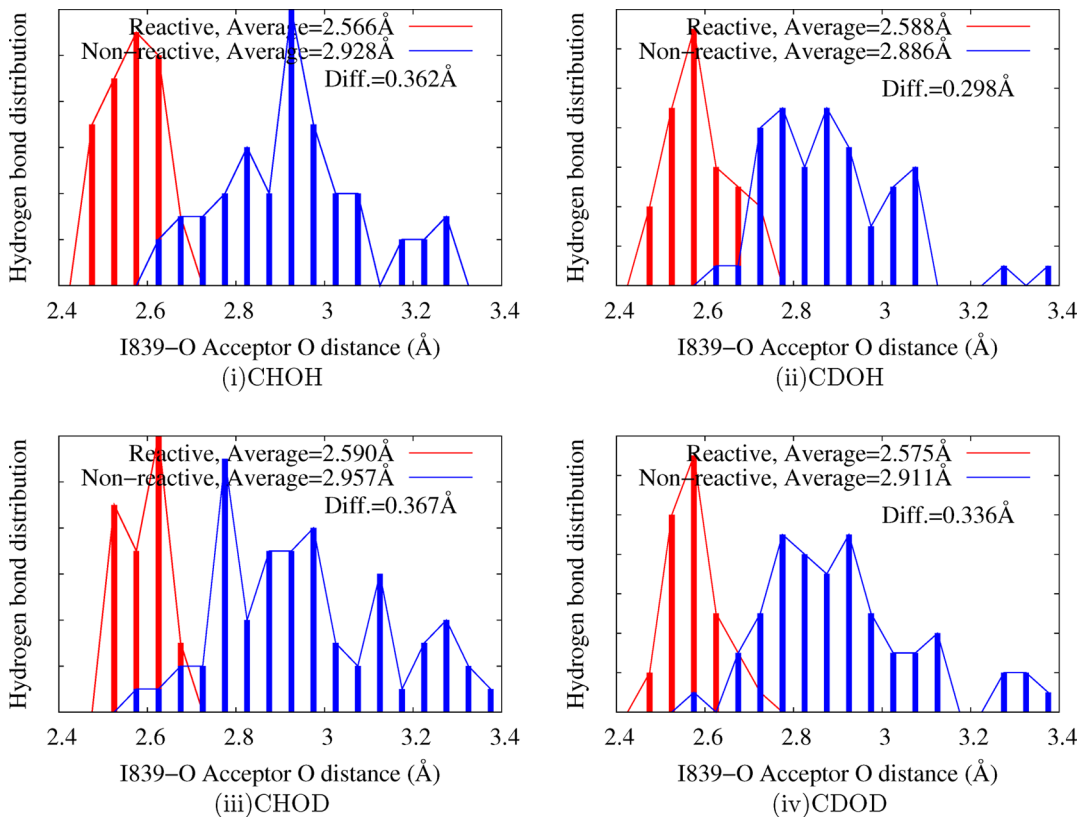


**Figure 7.** Distribution of hydrogen bonded distances between the isoleucine oxygen and acceptor oxygen. In each case, the hydrogen bond distance distribution is shorter and narrower for the reactive simulations where the hydrogen bonds are noted to be very strong based on the distances.

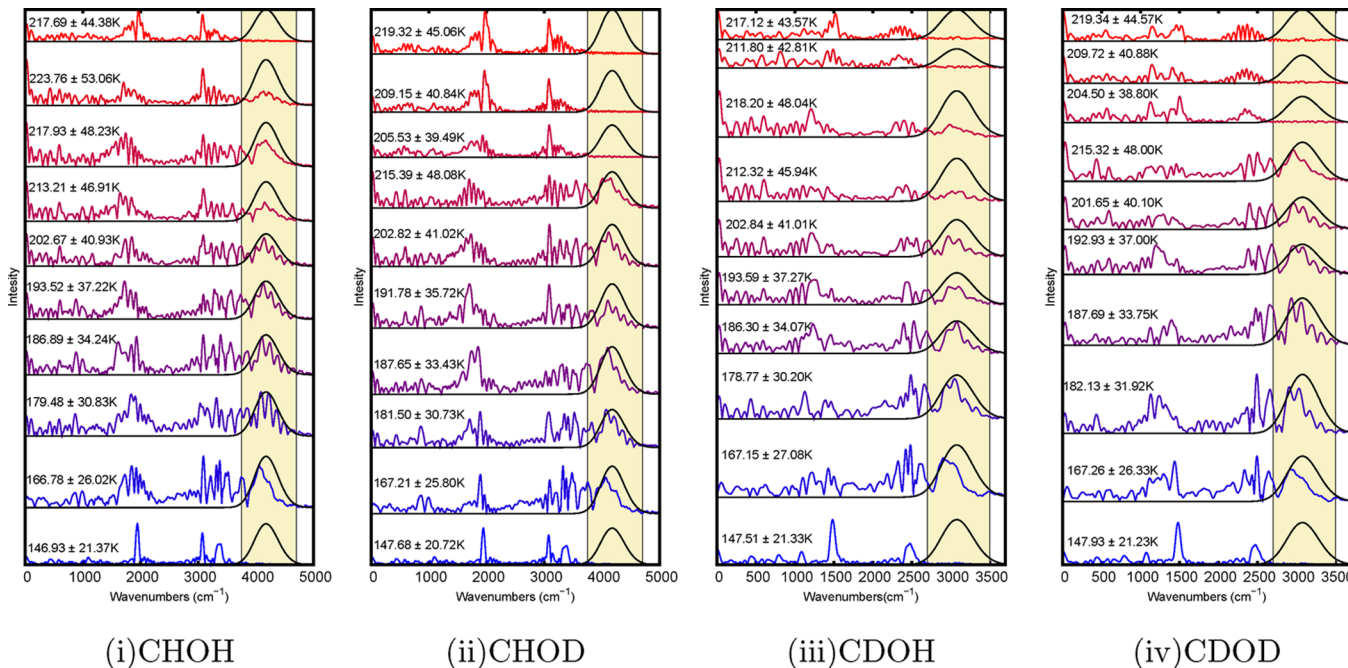


**Figure 8.** The vertical axes in each case represent  $C_i(\omega)$  contributions from the donor  $C_{11}-X$  stretch mode for the four isotopic variants. Note that it is only the productive simulations that show a spectral feature in the highlighted window. Compare with results in Figure 5. The skew-Gaussian weighting function,  $\mathcal{G}^{[\omega_1, \omega_2]}(\omega)$ , in eq 9 is also shown.

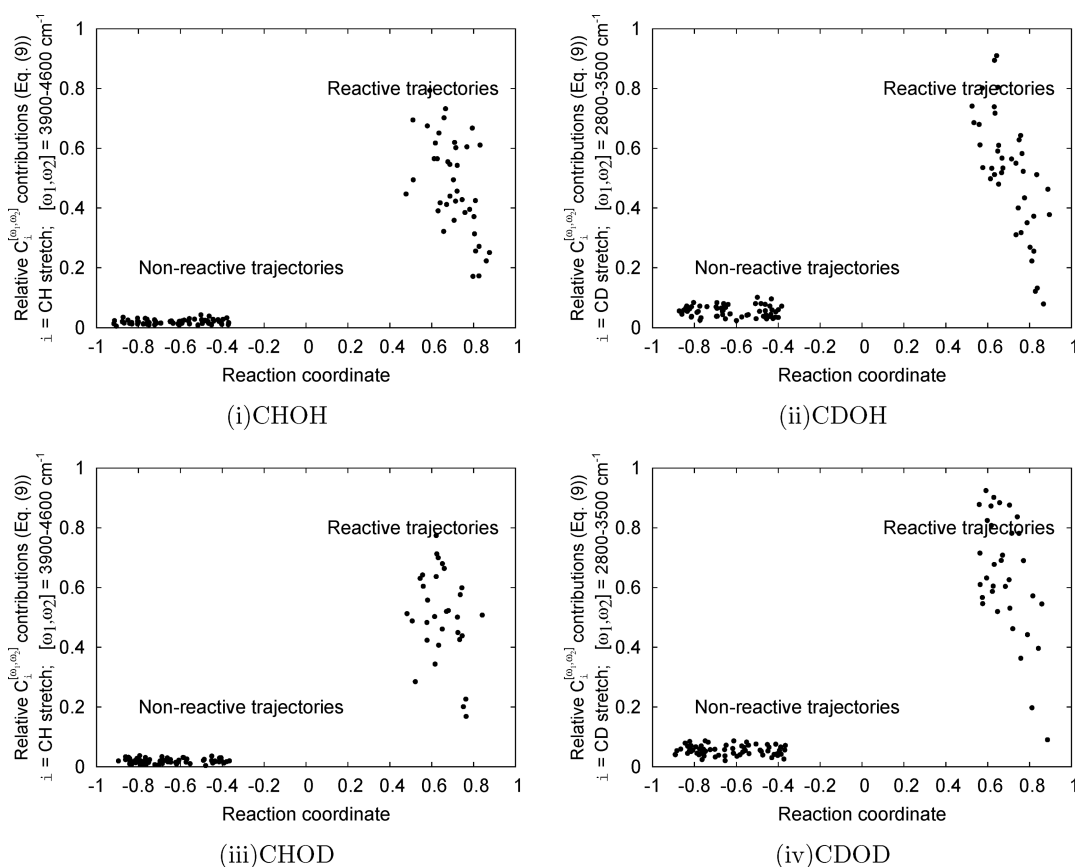


**Figure 9.** Distribution of  $C_i^{[\omega_1, \omega_2]}$  (see eq 9) where  $i$  is chosen to be the  $C_{11}$ -X stretch displayed in Figure 11 for all isotopologue. Clearly there is a large separation between contributions toward productive as opposed to nonproductive trajectories. We have also quantitatively confirmed this separation using Welch's  $t$  test<sup>121,122</sup> to contrast between the distribution of  $C_i^{[\omega_1, \omega_2]}$  for the productive and nonproductive simulations.

simulations and absent for others. For instance, in the CHOH system, this broad feature is present for all simulations except

for simulations with average nuclear kinetic energy corresponding to 146.93 K and 217.69 K (see Figure 8i top and bottom

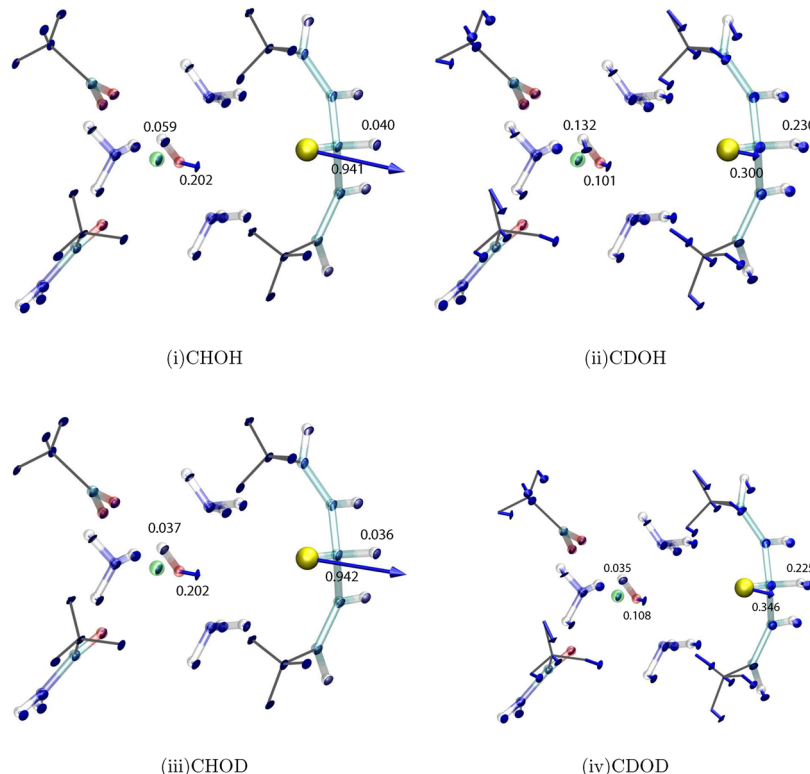


**Figure 10.** Most significant left singular vector from the singular value decomposition discussed in section IIB. Also shown are the relative magnitudes of fluctuation for the primary and secondary donor CH hydrogens, and acceptor OH group. For the primary deuterated systems in parts ii and iv, the secondary donor CH hydrogen is almost as labile as the transferring hydrogen itself for the productive simulations. This appears to indicate a greater vibrational coupling between the transferring deuteron and secondary CH hydrogen.

plots). These two simulations are the only two nonproductive simulations within this displayed set as is clear upon comparison with Figure Si. This trend is indicative of the fact that a distinct broad feature is observed when the simulations are productive and absent for nonproductive simulations. This correlation between the presence of a broad peak for productive simulations is also consistently observed for the remaining isotopic simulations.

As usual, to confirm that the effect described above is statistically significant, we compute  $C_i^{[\omega_1, \omega_2]}$  (see eq 9) inside the highlighted spectral window in Figures 8 for the entire set of 400 simulations. The weight function,  $\mathcal{G}^{[\omega_1, \omega_2]}(\omega)$ , is also shown in Figure 8. The results are presented in Figure 9. Clearly, the net contribution from  $C_i^{[\omega_1, \omega_2]}$  is well separated in all cases between reactive and nonreactive trajectories. Specifically, the  $C_i^{[\omega_1, \omega_2]}$  contributions are much larger in magnitude for the productive trajectories. Thus, the amount of energy in this spectral region is significantly different for the productive simulations as compared to the nonproductive simulations. (Note that  $|C_i^{[\omega_1, \omega_2]}|^2$  is proportional to the kinetic energy of the system in  $[\omega_1, \omega_2]$ .)

It must be emphasized that while our analysis here is based on the C<sub>11</sub>-X stretch corresponding to the reactant geometry and the corresponding C<sub>i</sub><sup>[ω<sub>1</sub>, ω<sub>2</sub>]</sup> coefficients, our results are not sensitive to this choice. The reason is as follows: First, the distribution of total kinetic energy, in the frequency representation, that is  $\mathcal{F}_\nu(\omega)$  in eq 3, is different in the noted frequency range of ~3900–4600 cm<sup>-1</sup> region for CHOX systems and ~2800–3500 cm<sup>-1</sup> region for CDOX systems, for productive and nonproductive results. This is a result

independent of coordinate systems. We then probe the portions of active site concerted motion that have significant differences in this same spectral range and find the C<sub>11</sub>-X stretch noted here to be an important player. It should, however, be noted that other modes, (obtained from other coordinate systems, presumably obtained by constructing vibrational modes from other geometries) that have significant overlap with the C<sub>11</sub>-X direction here will also show similar characteristics.

**D. “Effective” Dynamic Modes Computed from Singular Value Decomposition of the  $\nu_g^{[\omega_1, \omega_2]}$  Vectors in Eq 10 and Their Implication to Secondary Isotope Effects.** In section IIIC, we utilized the contributions from harmonic modes to the dynamics to further probe productive and nonproductive simulations. Here, we construct composite modes that are obtained from a singular value decomposition of the  $\nu_g^{[\omega_1, \omega_2]}$  as discussed in section IIB. The significant singular ( $U$ ) vectors represent the dominant composite modes that contribute to the broad feature in the  $\sim 3900\text{--}4600\text{ cm}^{-1}$  region for the CHOX systems and  $\sim 2800\text{--}3500\text{ cm}^{-1}$  region for the CDOX systems (Figure 8).

The most prominent singular-vectors (corresponding to the largest singular value) for all isotopic systems from the productive simulations are presented in Figure 10. In case of the CHOX systems, the largest fluctuation is observed along the C<sub>11</sub>–H direction. However, unlike the case of the harmonic modes (see Figure 11 in Appendix B), this mode is mixed with (a) the acceptor oxygen motion perpendicular to the linoleic acid axis (Figure 10, parts i and iii). In addition there is a small acceptor OH wag contribution. In Figure 10, the extent of these vibrations can be gauged by the size of the vectors, with relevant magnitudes labeled. For the CDOX systems, the C<sub>11</sub>–

D stretch contribution is substantially lower. This is balanced by a larger contribution from the linoleic acid modes. (See Figure 10, parts ii and iv.) One may contrast this behavior with the corresponding result for the harmonic case as seen in Figure 11 in Appendix B. Within the harmonic approximation the  $C_{11}$ -X stretch modes for CHO<sub>X</sub> are coupled with peripheral linoleic acid C–H stretch modes and this coupling disappears during the productive dynamics trajectories which include all anharmonic contributions. The opposite trend is observed for CDO<sub>X</sub>. Finally, the acceptor oxygen and acceptor OH wag contributions are similar for CDOD but the acceptor OH wag shows a greater contribution for CDOH.

It is also interesting to distinguish the flexibility of the secondary proton attached to the  $C_{11}$ -carbon for the CHO<sub>X</sub> and CDO<sub>X</sub> systems. It is noted from Figure 10 that the secondary  $C_{11}$ -proton is much more labile (by a factor of 5–6) for the CDO<sub>X</sub> systems. This definitely indicates that the motion of the secondary  $C_{11}$ -proton is much more tightly coupled to the D-transfer process as compared to the H-transfer process. The fact that such coupling is enhanced for the D-transfer case is consistent with the results seen in ref 28, where Knapp, Rickert and Klinman noted that the secondary kinetic isotope effect at the  $C_{11}$  position was greater (by a factor of 2) when the transferring species was deuterium as compared to a protium.

#### IV. CONCLUSIONS

Hydrogen bonds and hydrogen transfer reactions play a significant role in a wide variety of systems.<sup>123–130</sup> In recent years, several studies have suggested the significance of hydrogen tunneling in such problems.<sup>4–15</sup> In this publication we probe the facilitating active site molecular perturbations that may participate in the H/D transfer event in the enzyme soybean lipoxygenase-1 (SLO-1). We have employed a recently developed rare-events sampling approach<sup>47</sup> and we consider four different isotopologues involving the transferring hydrogen atom and an acceptor side hydroxyl hydrogen atom. In addition, we have also considered all the vibrational coupling arising from the donor side secondary  $C_{11}$ H hydrogen. While the latter (secondary  $C_{11}$ H hydrogen) has been known to yield nonclassical secondary isotope effects, the former (acceptor side OH hydrogen), we find, is involved in a hydrogen bond with the backbone I839 carbonyl group that is concomitant with the H/D transfer event. We find that the participation of the acceptor OH makes for a particularly interesting story with regards to facile hydrogen transfer. As a result of participation of the acceptor O–H–I839 hydrogen bond, initial increase in the average kinetic energy in the system yields an increase in reaction probability. However, this only follows until the point with the stated hydrogen bond weakens, at which point the reaction probability starts reducing with increasing average kinetic energy. Further increase in kinetic energy then results in an increase in reaction probability. This leads to zigzag, nonmonotonic, behavior of the reaction probability with system kinetic energy. On the basis of these results, we predict that an I839 → A839 or an I839 → V839 mutation would modify the bulkiness of hydrogen the bonding residue. This would allow more flexibility in the secondary hydrogen bond formation and adversely affect the reaction rate.

The second significant result in this paper pertains to the participation of vibrational modes that facilitate H/D transfer. For this purpose, we introduce a method that ascertains the vibrational contributions by factorizing frequency dependent

dynamical information in terms of molecular vibrational modes. In this case, we find that (a) deuterium transfer is more strongly coupled to the linoleic acid vibrations as compared to hydrogen transfer, (b) the secondary  $C_{11}$ H hydrogen is especially labile (by a factor of 5–6) during deuterium transfer as compared to hydrogen transfer, and (c) the ligand groups on the acceptor side also much more labile during deuterium transfer as compared to hydrogen transfer. It is instructive to note that in ref 28. Rickert and Klinman have found that there may exist an abnormal secondary isotope effect involving the  $C_{11}$ H hydrogen during deuterium transfer. (Such an abnormal secondary isotope effect was absent in the case of hydrogen transfer.) This result appears to be consistent with our vibrational coupling results noted above. Many body quantum nuclear effects will be studied in future publications.

#### ■ APPENDIX A: A BRIEF INTRODUCTION TO RARE-EVENTS SAMPLING BASED ON AB INITIO MOLECULAR DYNAMICS

As outlined in ref 47, we modify the atom-centered density-matrix propagation (ADMP) extended Lagrangian<sup>95–99,101,120,130–141</sup> to include “bath variables”,  $\tilde{\mathbf{R}}$ , that couple to a chosen set of nuclear degrees of freedom through a coupling potential,  $\eta$ , according to

$$\begin{aligned} \mathcal{L} = & \frac{1}{2} \text{Tr}[\mathbf{V}^T \mathbf{M} \mathbf{V}] + \frac{1}{2} \text{Tr}([\mu^{1/4} \mathbf{W} \mu^{1/4}]^2) \\ & + \frac{1}{2} \text{Tr}[\tilde{\mathbf{V}}^T \tilde{\mathbf{M}} \tilde{\mathbf{V}}] - E(\mathbf{R}, \mathbf{P}) - \eta(\mathbf{R}; \tilde{\mathbf{R}}) \\ & - \text{Tr}[\Lambda(\mathbf{P}\mathbf{P} - \mathbf{P})] \end{aligned} \quad (\text{A1})$$

Here  $\mathbf{M}$ ,  $\mathbf{R}$ , and  $\mathbf{V}$  are the nuclear masses, atomic positions and velocities. The quantities  $\tilde{\mathbf{M}}$ ,  $\tilde{\mathbf{R}}$ , and  $\tilde{\mathbf{V}}$  are the masses, positions and velocities of the family of fictitious, bath particles, and the function  $E(\mathbf{R}, \mathbf{P})$  is the *ab initio* potential energy function. This potential energy is a function of the single-particle electronic density matrix,  $\mathbf{P}$  and nuclear positions,  $\mathbf{R}$ . The bath variables do not directly affect  $E(\mathbf{R}, \mathbf{P})$  but have an indirect role through  $\mathbf{R}$ . An ONIOM<sup>79</sup> based QM/MM description is used for  $E(\mathbf{R}, \mathbf{P})$ . The full system is divided into *model* and *real* systems for the 2-layer ONIOM procedure employed in this work. The calculation at the highest level of theory is performed on the chemically reactive part of the system and

$$E(\mathbf{R}, \mathbf{P}) \rightarrow E^{\text{IMOMM}}(\mathbf{R}) = E_{\text{real}}^{\text{MM}} - E_{\text{mod el}}^{\text{MM}} + E_{\text{mod el}}^{\text{QM}} \quad (\text{A2})$$

If chemical bonds intersect the boundary between two layers, link atoms are used to saturate the dangling valencies of the smaller system.<sup>142</sup> The positions of link atoms are uniquely determined based on the connectivity of the system, which makes conservative dynamics possible.<sup>95</sup> Thus, the selected atoms and additional link atoms of each system are influenced by the properties of the atoms in the larger systems.

The quantity  $\eta(\mathbf{R}; \tilde{\mathbf{R}})$  in eq A1 is a coupling or tethering constraint on  $\mathbf{R}$  through introduction of  $\tilde{\mathbf{R}}$  and the function also defines the subset of particles in  $\mathbf{R}$  that are influenced by the constraint. We employ a harmonic tethering constraint,

$$\eta(\mathbf{R}; \tilde{\mathbf{R}}) \equiv \text{Tr}[(\mathbf{R} - \tilde{\mathbf{R}})^T \mathbf{K}(\mathbf{R} - \tilde{\mathbf{R}})] \quad (\text{A3})$$

and the Euler–Lagrange equations of motion are

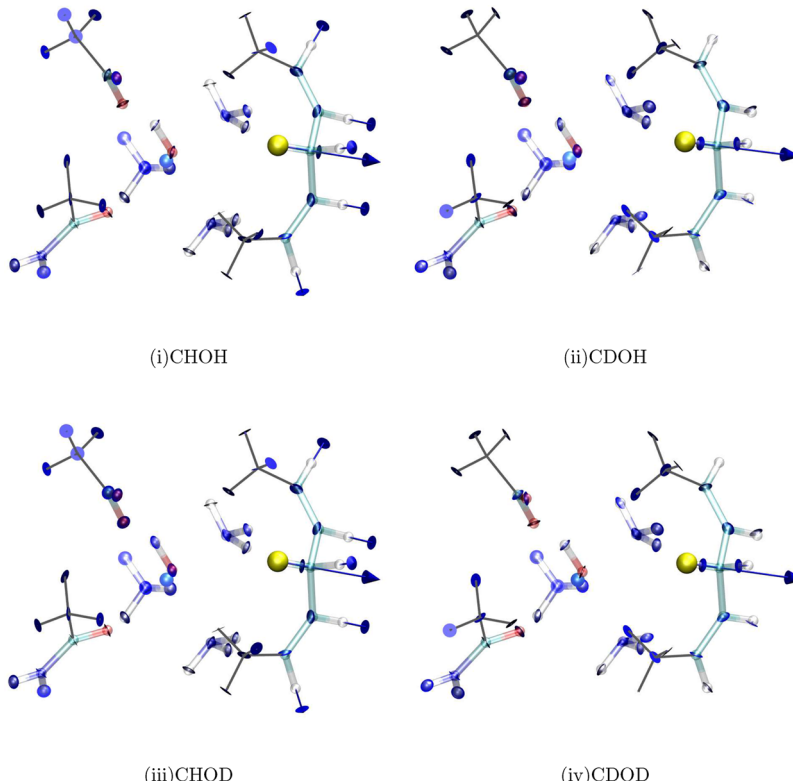


**Figure 11.** Donor  $C_{11}$ -X stretch modes within the harmonic approximation: (a) CHO<sub>H</sub>, 3165.78 cm<sup>-1</sup>; (b) CDO<sub>H</sub>, 2320.20 cm<sup>-1</sup>; (c) CHOD, 3165.41 cm<sup>-1</sup>; (d) CDOD, 2320.24 cm<sup>-1</sup>. For CHO<sub>X</sub> systems, within the harmonic approximation, the pure  $C_{11}$ -H stretch is coupled with linoleic acid peripheral pure C-H stretch modes. This coupling is absent in the donor  $C_{11}$ -X stretch mode for CDO<sub>X</sub> systems.

$$\mathbf{M} \frac{d^2\mathbf{R}}{dt^2} = -\frac{\partial E(\mathbf{R}, \mathbf{P})}{\partial \mathbf{R}}_p - \frac{1}{2}[(\mathbf{R} - \tilde{\mathbf{R}})^T \mathbf{K} + \mathbf{K}(\mathbf{R} - \tilde{\mathbf{R}})] \quad (A4)$$

$$\tilde{\mathbf{M}} \frac{d^2\tilde{\mathbf{R}}}{dt^2} = \frac{1}{2}[(\mathbf{R} - \tilde{\mathbf{R}})^T \mathbf{K} + \mathbf{K}(\mathbf{R} - \tilde{\mathbf{R}})] \quad (A5)$$

$$\mu^{1/2} \frac{d^2\mathbf{P}}{dt^2} \mu^{1/2} = -\frac{\partial E(\mathbf{R}, \mathbf{P})}{\partial \mathbf{P}}_R - \Lambda \mathbf{P} - \mathbf{P} \Lambda + \Lambda \quad (A6)$$

These are integrated using the velocity Verlet scheme.<sup>143</sup> Since the force on the classical particles (first term on right side of eq A4) is augmented by additional forces from  $\tilde{\mathbf{R}}$  (second term on right side of eq A4) the dynamics of the  $\tilde{\mathbf{R}}$  is utilized to bias the dynamics of the system and access regions in phase space that are not readily sampled otherwise.

## APPENDIX B: THE CRITICAL HARMONIC MODES THAT CONTRIBUTE TO REACTIVITY

As noted in section IIIC in the publication, the  $C_{11}$ -X (the symbol "X" refers to the transferring hydrogen or deuterium) harmonic stretch contributes critically to the hydrogen transfer process. The  $C_{11}$ -X stretch harmonic modes are displayed in Figure 11. These are the modes used in the main paper to resolve differences between productive and non-productive trajectories. For the case of CHO<sub>X</sub>, this harmonic mode is comprised of several local modes including the pure donor  $C_{11}$ -H stretch mode which is coupled with the linoleic acid peripheral C-H stretch motion (Figure 11, parts i and iii). In the deuterated CDO<sub>X</sub> system, on the other hand, the donor  $C_{11}$ -D harmonic stretch mode at 2320.20 cm<sup>-1</sup> is significantly red-shifted with respect to the corresponding mode of CHO<sub>X</sub>

(3165.78 cm<sup>-1</sup>) and hence exhibits significantly less coupling with the linoleic acid peripheral C-H stretch motion (Figure 11, parts ii and iv). Similarly, there is minimal coupling to the acceptor side OH hydrogen in all cases. These couplings are substantially modified during the reactive process as seen in Figure 10 in the paper.

To summarize, in comparison with CDO<sub>H</sub> normal modes, CHO<sub>H</sub> normal modes display greater coupling between donor  $C_{11}$ -H and other Linoleic acid modes. Qualitatively similar trends are observed for normal modes of CHOD and CDOD systems. In addition to the  $C_{11}$ -X stretch harmonic modes there are other modes that contribute significantly to the ~3900–4600 cm<sup>-1</sup> region for CHO<sub>X</sub> systems and ~2800–3500 cm<sup>-1</sup> region for CDO<sub>X</sub> systems. We only probe the effect of the  $C_{11}$ -X in this publication.

## AUTHOR INFORMATION

### Corresponding Author

\*(S.S.I.) E-mail: iyengar@indiana.edu.

### Author Contributions

<sup>†</sup>These two authors contributed in equal amount to this publication.

### Notes

The authors declare no competing financial interest.

## ACKNOWLEDGMENTS

This research is supported by National Institute of Health Grant GM-087475 (SSI) and National Science Foundation Grant NSF CHE-1058949 (SSI).

## ■ REFERENCES

- (1) Hynes, J. T.; Klinman, J. P.; Limbach, H.-H.; Schowen, R. L., Eds. *Hydrogen-Transfer Reactions*; Wiley-VCH: Weinheim, Germany, 2007.
- (2) Isaacs, N. *Physical Organic Chemistry*; Longman Scientific and Technical: Essex, U.K., 1995.
- (3) Sheridan, R. Quantum Mechanical Tunneling in Organic Reactive Intermediates, in *Reviews of Reactive Intermediate Chemistry*; Platz, M., Moss, R. A., Maitland Jones, J., Eds.; Wiley-Interscience: Hoboken, NJ, 2007.
- (4) Nagel, Z.; Klinman, J. Tunneling and Dynamics in Enzymatic Hydride Transfer. *Chem. Rev.* **2006**, *106* (8), 3095–3118.
- (5) Hammes-Schiffer, S.; Benkovic, S. J. Relating Protein Motion to Catalysis. *Annu. Rev. Biochem.* **2006**, *75*, 519.
- (6) Benkovic, S. J.; Hammes-Schiffer, S. Biochemistry - Enzyme Motions Inside and Out. *Science* **2006**, *312*, 208.
- (7) Bahnsen, B. J.; Colby, T. D.; Chin, J. K.; Goldstein, B. M.; Klinman, J. P. A Link Between Protein Structure and Enzyme Catalyzed Hydrogen Tunneling. *Proc. Natl. Acad. Sci. U.S.A.* **1997**, *94*, 12797.
- (8) Garcia-Viloca, M.; Gao, J.; Karplus, M.; Truhlar, D. G. How Enzymes Work: Analysis by Modern Rate Theory and Computer Simulations. *Science* **2004**, *303*, 5655.
- (9) Olsson, M. H. M.; Siegbahn, P. E. M.; Warshel, A. Simulations of the Large Kinetic Isotope Effect and the Temperature Dependence of the Hydrogen Atom Transfer in Lipoxygenase. *J. Am. Chem. Soc.* **2004**, *126*, 2820–2828.
- (10) Antoniou, D.; Basner, J.; Nunez, S.; Schwartz, S. Computational and Theoretical Methods to Explore the Relation Between Enzyme Dynamics And Catalysis. *Chem. Rev.* **2006**, *106* (8), 3170–3187.
- (11) Klinman, J. P. Dynamic Barriers and Tunneling. New Views of Hydrogen Transfer in Enzyme Reactions. *Pure Appl. Chem.* **2003**, *75*, 601.
- (12) Liang, Z. X.; Klinman, J. P. Structural Bases of Hydrogen Tunneling in Enzymes: Progress and Puzzles. *Curr. Opin. Struct. Biol.* **2004**, *14*, 648.
- (13) Pu, J. Z.; Gao, J. L.; Truhlar, D. G. Multidimensional Tunneling, Recrossing, and the Transmission Coefficient for Enzymatic Reactions. *Chem. Rev.* **2006**, *106*, 3140–3169.
- (14) Gao, J. L.; Ma, S. H.; Major, D. T.; Nam, K.; Pu, J. Z.; Truhlar, D. G. Mechanisms and Free Energies of Enzymatic Reactions. *Chem. Rev.* **2006**, *106*, 3188–3209.
- (15) Kamerlin, S.; Mavri, J.; Warshel, A. Examining the Case for the Effect of Barrier Compression on Tunneling, vibrationally Enhanced Catalysis, Catalytic Entropy and Related Issues. *FEBS Lett.* **2010**, *584*, 2759–2766.
- (16) Soudackov, A. V.; Hammes-Schiffer, S. Probing Nonadiabaticity in the Proton-Coupled Electron Transfer Reaction Catalyzed by Soybean Lipoxygenase. *J. Phys. Chem. Lett.* **2014**, *5*, 3274–3278.
- (17) Klinman, J. P. Dynamically Achieved Active Site Precision in Enzyme Catalysis. *Acc. Chem. Res.* **2015**, *48*, 449456.
- (18) Glickman, M. H.; Wiseman, J. S.; Klinman, J. P. Extremely Large Isotope Effects in the Soybean Lipoxygenase-Linoleic Acid Reaction. *J. Am. Chem. Soc.* **1994**, *116*, 793.
- (19) Jonsson, T.; Glickman, M. H.; Sun, S. J.; Klinman, J. P. Experimental Evidence for Extensive Tunneling of Hydrogen in the Lipoxygenase Reaction: Implications for Enzyme Catalysis. *J. Am. Chem. Soc.* **1996**, *118*, 10319.
- (20) Rickert, K. W.; Klinman, J. P. Nature of Hydrogen Transfer in Soybean Lipoxygenase 1: Separation of Primary and Secondary Isotope Effects. *Biochemistry* **1999**, *38*, 12218.
- (21) Meyer, M. P.; Klinman, J. P. Modeling Temperature Dependent Kinetic Isotope Effects for Hydrogen Transfer in a series of Soybean Lipoxygenase Mutants: the Effect of Anharmonicity upon Transfer Distance. *Chem. Phys.* **2005**, *319*, 283.
- (22) Hatcher, E.; Soudackov, A. V.; Hammes-Schiffer, S. Proton-Coupled Electron Transfer in Soybean Lipoxygenase. *J. Am. Chem. Soc.* **2004**, *126*, 5763–5775.
- (23) Olsson, M. H. M.; Siegbahn, P. E. M.; Warshel, A. Simulating Large Nuclear Quantum Mechanical Corrections in Hydrogen Atom Transfer Reactions in Metalloenzymes. *J. Biol. Inorg. Chem.* **2004**, *9*, 96–99.
- (24) Siebrand, W.; Smedarchina, Z. Temperature Dependence of Kinetic Isotope Effects for Enzymatic Carbon-Hydrogen Bond Cleavage. *J. Phys. Chem. B* **2004**, *108*, 4185.
- (25) Lehnert, N.; Solomon, E. I. Density-Functional Investigation on the Mechanism of H-atom Abstraction by Lipoxygenase. *J. Biol. Inorg. Chem.* **2003**, *8*, 294.
- (26) Knapp, M. J.; Seebeck, F. P.; Klinman, J. P. Steric Control of Oxygenation Regiochemistry in Soybean Lipoxygenase-1. *J. Am. Chem. Soc.* **2001**, *123*, 2931.
- (27) Glickman, M. H.; Wiseman, J. S.; Klinman, J. P. Extremely Large Isotope Effects in the Soybean Lipoxygenase-Linoleic Acid Reaction. *J. Am. Chem. Soc.* **1994**, *116*, 793–794.
- (28) Knapp, M. J.; Rickert, K.; Klinman, J. P. Temperature-Dependent Isotope Effects in Soybean Lipoxygenase-1: Correlating Hydrogen Tunneling with Protein Dynamics. *J. Am. Chem. Soc.* **2002**, *124*, 3865.
- (29) Alhambra, C.; Corchado, J.; Sanchez, M. L.; Garcia-Viloca, M.; Gao, J.; Truhlar, D. G. Canonical Variational Theory for Enzyme Kinetics with the Protein Mean Force and Multidimensional Quantum Mechanical Tunneling Dynamics. Theory and Application to Liver Alcohol Dehydrogenase. *J. Phys. Chem. B* **2001**, *105*, 11326–11340.
- (30) Garcia-Viloca, M.; Alhambra, C.; Truhlar, D. G.; Gao, J. L. Hydride Transfer Catalyzed by Xylose Isomerase: Mechanism and Quantum Effects. *J. Comput. Chem.* **2003**, *24*, 177–190.
- (31) Gao, J. Hybrid Quantum and Molecular Mechanical Simulations: An Alternative Avenue to Solvent Effects in Organic Chemistry. *Acc. Chem. Res.* **1996**, *29*, 298.
- (32) Hatcher, E.; Soudackov, A. V.; Hammes-Schiffer, S. Proton-Coupled Electron Transfer in Soybean Lipoxygenase: Dynamical Behavior and Temperature Dependence of Kinetic Isotope Effects. *J. Am. Chem. Soc.* **2007**, *129*, 187.
- (33) Hammes-Schiffer, S. Quantum-Classical Simulation Methods for Hydrogen Transfer in Enzymes: A Case Study of Dihydrofolate Reductase. *Curr. Opin. Struct. Biol.* **2004**, *14*, 192–201.
- (34) Edwards, S.; Soudackov, A.; Hammes-Schiffer, S. Impact of Distal Mutation on Hydrogen Transfer Interface and Substrate Conformation in Soybean Lipoxygenase. *J. Phys. Chem. B* **2010**, *114*, 6653–6660.
- (35) Meyer, M. P.; Tomchick, D. R.; Klinman, J. P. Enzyme Structure and Dynamics Affect Hydrogen Tunneling: The Impact of a Remote Side Chain (I553) in Soybean Lipoxygenase-1. *Proc. Natl. Acad. Sci. U.S.A.* **2008**, *105*, 1146.
- (36) Warshel, A.; Sharma, P.; Kato, M.; Xiang, Y.; Liu, H.; Olsson, M. Electrostatic Basis for Enzyme Catalysis. *Chem. Rev.* **2006**, *106* (8), 3210–3235.
- (37) Cao, J.; Voth, G. A. The Formulation of Quantum Statistical Mechanics Based on the Feynman Path Centroid Density. IV. Algorithms for Centroid Molecular Dynamics. *J. Chem. Phys.* **1994**, *101*, 6168.
- (38) Jang, S.; Voth, G. A. A Derivation of Centroid Molecular Dynamics and Other Approximate Time Evolution Methods for Path Integral Centroid Variables. *J. Chem. Phys.* **1999**, *111*, 2371.
- (39) Warshel, A.; Weiss, R. M. An Empirical Valence Bond Approach for Comparing Reactions in Solutions and in Enzymes. *J. Am. Chem. Soc.* **1980**, *102*, 6218.
- (40) Chang, Y.-T.; Miller, W. H. An Empirical Valence Bond Model for Constructing Global Potential Energy Surfaces for Chemical Reactions of Polyatomic Molecular Systems. *J. Phys. Chem.* **1990**, *94*, 5884.
- (41) Day, T. J. F.; Soudackov, A. V.; Cuma, M.; Schmidt, U. W.; Voth, G. A. A Second Generation Multistate Empirical Valence Bond Model for Proton Transport in Water. *J. Chem. Phys.* **2002**, *117*, 5839.
- (42) Wang, F.; Voth, G. A. A Linear-Scaling Self-Consistent Generalization of the Multistate Empirical Valence Bond Method for Multiple Excess Protons in Aqueous Systems. *J. Chem. Phys.* **2005**, *122*, 144105.

- (43) Miller, W. H.; Schwartz, S. D.; Tromp, J. W. Quantum Mechanical Rate Constants for Bimolecular Reactions. *J. Chem. Phys.* **1983**, *79*, 4889.
- (44) Kuznetsov, A. M.; Ulstrup, J. Proton and Hydrogen Atom Tunnelling in Hydrolytic and Redox Enzyme Catalysis. *Can. J. Chem.* **1999**, *77*, 1085.
- (45) Iyengar, S. S.; Sumner, I.; Jakowski, J. Hydrogen Tunneling in an Enzyme Active Site: a Quantum Wavepacket Dynamical Perspective. *J. Phys. Chem. B* **2008**, *112*, 7601–7613.
- (46) Sumner, I.; Iyengar, S. S. Analysis of Hydrogen Tunneling in an Enzyme Active Site Using von Neumann Measurements. *J. Chem. Theory Comput.* **2010**, *6*, 1698.
- (47) Phatak, P.; Sumner, I.; Iyengar, S. S. Gauging the Flexibility of the Active Site in Soybean Lipoxygenase-1 (SLO-1) Through an Atom-Centered Density Matrix Propagation (ADMP) Treatment that Facilitates the Sampling of Rare Events. *J. Phys. Chem. B* **2012**, *116*, 10145.
- (48) Jarzynski, C. Equalities and Inequalities: Irreversibility and the Second Law of Thermodynamics at the Nanoscale. *Annu. Rev. Condens. Matter Phys.* **2011**, *2*, 329–351.
- (49) Jarzynski, C. Nonequilibrium Equality for Free Energy Differences. *Phys. Rev. Lett.* **1997**, *78* (14), 2690–2693.
- (50) Jarzynski, C. Equilibrium free-energy differences from non-equilibrium measurements: A Master-Equation Approach. *Phys. Rev. E* **1997**, *56*, 5018–5035.
- (51) Ilan, B.; Tajkhorshid, E.; Schulten, K.; Voth, G. A. The Mechanism of Proton Exclusion in Aquaporin Channels. *Proteins: Struct., Funct., Bioinf.* **2004**, *55*, 223–228.
- (52) Park, S.; Khalili-Araghi, F.; Tajkhorshid, E.; Schulten, K. Free Energy Calculation from Steered Molecular Dynamics Simulations Using Jarzynski's Equality. *J. Chem. Phys.* **2003**, *119*, 3559–3566.
- (53) Presse, S.; Silbey, R. Ordering of Limits in the Jarzynski Equality. *J. Chem. Phys.* **2006**, *124*, 054117.
- (54) Presse, S.; Silbey, R. J. Memory Effects on the Convergence Properties of the Jarzynski Equality. *Phys. Rev. E* **2006**, *74*, 061105.
- (55) Liphardt, J.; Dumont, S.; Smith, S.; Tinoco, I.; Bustamante, C. Equilibrium Information from Nonequilibrium Measurements in an Experimental Test of Jarzynski's Equality. *Science* **2002**, *296*, 1832–1835.
- (56) MacFadyen, J.; Andricioaei, I. A Skewed-Momenta Method to Efficiently Generate Conformational-Transition Trajectories. *J. Chem. Phys.* **2005**, *123*, 074107.
- (57) Park, S.; Schulten, K. Calculating Potentials of Mean Force from Steered Molecular Dynamics Simulations. *J. Chem. Phys.* **2004**, *120*, 5946.
- (58) Paci, E.; Karplus, M. Forced Unfolding of Fibronectin Type 3 Modules: An Analysis by Biased Molecular Dynamics Simulations. *J. Mol. Biol.* **1999**, *288*, 441.
- (59) Ensing, B.; Laio, A.; Parrinello, M.; Klein, M. L. A Recipe for the Computation of the Free Energy Barrier and the Lowest Free Energy Path of Concerted Reactions. *J. Phys. Chem. B* **2005**, *109*, 6676–6687.
- (60) Abrams, J. B.; Tuckerman, M. E. Efficient and Direct Generation of Multidimensional Free Energy Surfaces via Adiabatic Dynamics without Coordinate Transformations. *J. Phys. Chem. B* **2008**, *112*, 15742–15757.
- (61) Maragliano, L.; Vanden-Eijnden, E. A Temperature Accelerated Method for Sampling Free Energy and Determining Reaction Pathways in Rare Events Simulations. *Chem. Phys. Lett.* **2006**, *426*, 168–175.
- (62) Olander, R.; Elber, R. Calculation of Classical Trajectories with a Very Large Time Step: Formalism and Numerical Examples. *J. Chem. Phys.* **1996**, *105*, 9299.
- (63) Elber, R.; Ghosh, A.; Cardenas, A. Long Time Dynamics of Complex Systems. *Acc. Chem. Res.* **2002**, *35*, 396–403.
- (64) Elber, R.; Ghosh, A.; Cardenas, A. In *Bridging the Time Scales: Molecular Simulations for the Next Decade*; Nielaba, P., Mareschal, M., Ciccotti, G., Eds.; Springer Verlag: Berlin, 2002; pp 335–363.
- (65) Elber, R.; Ghosh, A.; Cardenas, A.; Stern, H. Bridging the Gap between Reaction Pathways, Long Time Dynamics and Calculation of Rates. *Adv. Chem. Phys.* **2003**, *126*, 93–129.
- (66) Elber, R. Long-Timescale Simulation Methods. *Curr. Opin. Struct. Biol.* **2005**, *15*, 151–156.
- (67) Passerone, D.; Parrinello, M. Action-Derived Molecular Dynamics in the Study of Rare Events. *Phys. Rev. Lett.* **87**102001.
- (68) Passerone, D.; Ceccarelli, M.; Parrinello, M. A Conceted Variational Strategy for Investigating Rare Events. *J. Chem. Phys.* **2003**, *118* (5), 2025–2032.
- (69) Elber, R.; Karplus, M. A Method for Determining Reaction Paths in Large Molecules: Application to Myoglobin. *Chem. Phys. Lett.* **1987**, *139* (5), 375–380.
- (70) Gillilan, R. E.; Wilson, K. R. Shadowing, Rare Events, and Rubber Bands - A Variational Verlet Algorithm for Molecular-Dynamics. *J. Chem. Phys.* **1992**, *97*, 1757–1772.
- (71) Henkelman, G.; Jonsson, H. Improved Tangent Estimate in the Nudged Elastic Band Method for Finding Minimum Energy Paths and Saddle Points. *J. Chem. Phys.* **2000**, *113*, 9978–9985.
- (72) Sørensen, M. R.; Voter, A. F. Temperature-Accelerated Dynamics for Simulation of Infrequent Events. *J. Chem. Phys.* **2000**, *112*, 9599.
- (73) Carter, E. A.; Ciccotti, G.; Hynes, J. T.; Kapral, R. Constrained Reaction Coordinate Dynamics for the Simulation of Rare Events. *Chem. Rev. Lett.* **1989**, *156*, 472.
- (74) Voter, A. F. A. Method for Accelerating the Molecular Dynamics Simulation of Infrequent Events. *J. Chem. Phys.* **1997**, *106*, 4665.
- (75) Voter, A. F. Hyperdynamics: Accelerated Molecular Dynamics of Infrequent Events. *Phys. Rev. Lett.* **1997**, *78*, 3908.
- (76) Warshel, A.; Levitt, M. Theoretical Studies of Enzymic Reactions: Dielectric, Electrostatic and Steric Stabilization of the Carbonium Ion in the Reaction of Lysozyme. *J. Mol. Biol.* **1976**, *103*, 227.
- (77) Singh, U. C.; Kollman, P. A. A Combined Ab Initio Quantum Mechanical and Molecular Mechanical Method for Carrying Out Simulations on Complex Molecular Systems: Applications to the  $\text{CH}_3\text{Cl} + \text{Cl}^-$  Exchange Reaction and Gas Phase Protonation of Polyethers. *J. Comput. Chem.* **1986**, *7*, 718.
- (78) Field, C.; Bash, P. A.; Karplus, M. A Combined Quantum Mechanical and Molecular Mechanical Potential for Molecular Dynamics Simulations. *J. Comput. Chem.* **1990**, *11*, 700.
- (79) Maseras, F.; Morokuma, K. A New "Ab Initio + Molecular Mechanics" Geometry Optimization Scheme of Equilibrium Structures and Transition States. *J. Comput. Chem.* **1995**, *16*, 1170–1179.
- (80) Ferenczy, G. G.; Rivail, J.-L.; Surjan, P. R.; Naray-Szabo, G. NDDO Fragment Self-Consistent Field Approximation for Large Electronic Systems. *J. Comput. Chem.* **1992**, *13*, 830.
- (81) Gao, J.; Amara, P.; Alhambra, C.; Field, M. A Generalized Hybrid Orbital (GHO) Method for the Treatment of Boundary Atoms in Combined QM/MM Calculations. *J. Phys. Chem. A* **1998**, *102*, 4714.
- (82) Zhang, Y.; Lee, T.-S.; Yang, W. A Pseudobond Approach to Combining Quantum Mechanical and Molecular Mechanical Methods. *J. Chem. Phys.* **1999**, *110*, 45.
- (83) Stanton, R. V.; Hartough, D. S.; Merz, K. M. An Examination of a Density Functional/Molecular Mechanical Coupled Potential. *J. Comput. Chem.* **1994**, *16*, 113.
- (84) Alhambra, C.; Byun, K.; Gao, J. The Geometry of Water in Liquid Water from Hybrid Ab Initio-Monte Carlo and Density Functional-Molecular Dynamics Simulations. In *Combined Quantum Mechanical and Molecular Mechanics Methods*; Gao, J., Thompson, M., Eds., ACS Symposium Series 712; American Chemical Society: Washington DC, 1998; p 35.
- (85) Reuter, N.; Dejaegere, A.; Maigret, B.; Karplus, M. Frontier Bonds in QM/MM Methods: A Comparison of Different Approaches. *J. Phys. Chem. A* **2000**, *104*, 1720.
- (86) Murphy, R. B.; Philipp, D. M.; Friesner, R. A. A Mixed Quantum Mechanics/Molecular Mechanics (QM/MM) Method for Large-Scale

- Modeling of Chemistry in Protein Environments. *J. Comput. Chem.* **2000**, *21*, 1442.
- (87) Woo, T. K.; P, M. M.; Deng, L.; Ziegler, T. In *Combined Quantum Mechanical and Molecular Mechanics Methods*; Gao, J., Thompson, M., Eds., ACS Symposium Series 712; American Chemical Society: Washington DC, 1998; p 128.
- (88) Laio, A.; VandeVondele, J.; Röthlisberger, U. A Hamiltonian Electrostatic Coupling Scheme for Hybrid Car-Parrinello Molecular Dynamics Simulations. *J. Chem. Phys.* **2002**, *116*, 6941–6947.
- (89) Eichinger, M.; Tavan, P.; Hutter, J.; Parrinello, M. A Hybrid Method for Solutes in Complex Solvents: Density Functional Theory Combined with Empirical Force Fields. *J. Chem. Phys.* **1999**, *110*, 10452.
- (90) Gordon, M. S.; Freitag, M. A.; Bandyopadhyay, P.; Jensen, J. H.; Kairys, V.; Stevens, W. J. The Effective Fragment Potential Method: A QM-Based MM Approach to Modeling Environmental Effects in Chemistry. *J. Phys. Chem. A* **2001**, *105*, 293–307.
- (91) Zhang, Y.; Lin, H.; Truhlar, D. Self-Consistent Polarization of the Boundary in the Redistributed Charge and Dipole Scheme for Combined Quantum-Mechanical and Molecular-Mechanical Calculations. *J. Chem. Theory Comput.* **2007**, *3* (4), 1378–1398.
- (92) Lin, H.; Truhlar, D. G. QM/MM: What Have We Learned Where Are We, and Where Do We Go from Here? *Theor. Chem. Acc.* **2007**, *117*, 185–199.
- (93) Toniolo, A.; Granucci, G.; Martinez, T. J. Conical Intersections in Solution: A QM/MM Study Using Floating Occupation Semi-empirical Configuration Interaction Wave Functions. *J. Phys. Chem. A* **2003**, *107*, 3822–3830.
- (94) Hratchian, H. P.; Parandekar, P. V.; Raghavachari, K.; Frisch, M. J.; Vreven, T. QM:QM Electronic Embedding Using Mulliken Atomic Charges: Energies and Analytic Gradients in an ONIOM Framework. *J. Chem. Phys.* **2008**, *128*, 034107.
- (95) Rega, N.; Iyengar, S. S.; Voth, G. A.; Schlegel, H. B.; Vreven, T.; Frisch, M. J. Hybrid Ab-Initio/Empirical Molecular Dynamics: Combining the ONIOM Scheme with the Atom-Centered Density Matrix Propagation (ADMP) Approach. *J. Phys. Chem. B* **2004**, *108*, 4210–4220.
- (96) Sumner, I.; Iyengar, S. S. Combining Quantum Wavepacket *Ab Initio* Molecular Dynamics (QWAIMD) with QM/MM and QM/QM Techniques: Implementation Blending ONIOM and Empirical Valence Bond Theory. *J. Chem. Phys.* **2008**, *129*, 054109.
- (97) Minor, W.; Steczko, J.; Stec, B.; Otwinskiowski, Z.; Bolin, J. T.; Walter, R.; Axelrod, B. Crystal Structure of Soybean Lipoygenase L-1 at 1.4 Å Resolution. *Biochemistry* **1996**, *35*, 10687–10701.
- (98) Li, X.; Oomens, J.; Eyler, J. R.; Moore, D. T.; Iyengar, S. S. Isotope Dependent, Temperature Regulated, Energy Repartitioning in a Low-Barrier, Short-Strong Hydrogen Bonded Cluster. *J. Chem. Phys.* **2010**, *132*, 244301.
- (99) Li, X.; Moore, D. T.; Iyengar, S. S. Insights from First Principles Molecular Dynamics Studies Towards Infra-Red Multiple-Photon and Single-Photon Action Spectroscopy: Case Study of the Proton-Bound Di-methyl Ether Dimer. *J. Chem. Phys.* **2008**, *128*, 184308.
- (100) Dietrick, S. M.; Iyengar, S. S. Constructing Periodic Phase Space Orbits from *Ab Initio* Molecular Dynamics Trajectories to Analyze Vibrational Spectra: Case Study of the Zundel ( $\text{H}_5\text{O}_2^+$ ) Cation. *J. Chem. Theory Comput.* **2012**, *8*, 4876.
- (101) Vimal, D.; Pacheco, A. B.; Iyengar, S. S.; Stevens, P. S. Experimental and *Ab Initio* Dynamical Investigations of the Kinetics and Intramolecular Energy Transfer Mechanisms for the OH+1,3-butadiene Reaction Between 263 and 423 K at Low Pressure. *J. Phys. Chem. A* **2008**, *112*, 7227–7237.
- (102) Fermi, E., Pasta, J. R., Ulam, S. *Studies of Non-Linear Problems. I.* Technical Report No. 1940, Los Alamos Report; 1955.
- (103) Robinson, P. J., Holbrook, K. A. *Unimolecular Reactions*; Wiley: New York, 1972.
- (104) Forst, W. *Theory of Unimolecular Reactions*; Academic Press: New York, 1973.
- (105) Jortner, J.; Levine, R. Photoselective Chemistry. *Adv. Chem. Phys.* **1981**, *47* (Part 1), 1–114.
- (106) Parmenter, C. S. Vibrational Energy Flow Within Excited Electronic States Of Large Molecules. *J. Phys. Chem.* **1982**, *86*, 1735.
- (107) Parmenter, C. S. Vibrational Redistribution Within Excited States Of Polyatomic Molecules. *Faraday Disc. Chem. Soc.* **1983**, *75*, 7–22.
- (108) Khundkar, L. R.; Zewail, A. H. Ultrafast Molecular Reaction Dynamics in Real-Time: Progress Over a Decade. *Annu. Rev. Phys. Chem.* **1990**, *41*, 15–60.
- (109) Uzer, T.; Miller, W. H. Theories of Intramolecular Vibrational-Energy Transfer. *Phys. Rep.* **1991**, *199*, 73–146.
- (110) Nesbitt, D. J.; Field, R. W. Vibrational Energy Flow in Highly Excited Molecules: Role of Intramolecular Vibrational Redistribution. *J. Phys. Chem.* **1996**, *100*, 12735–12756.
- (111) Gruebele, M. Mechanism and Control of Molecular Energy Flow: A Modeling Perspective. *Theor. Chem. Acc.* **2003**, *109*, 53–63.
- (112) Liu, Y.; Lohr, L. L.; Barker, J. R. Quasi-Classical Trajectory Simulations of Intramolecular Vibrational Energy Redistribution in  $\text{HONO}_2$  and  $\text{DONO}_2$ . *J. Phys. Chem. B* **2005**, *109*, 8304–8309.
- (113) Keshavamurthy, S. Dynamical Tunnelling in Molecules: Quantum Routes to Energy Flow. *Int. Rev. Phys. Chem.* **2007**, *26*, 521–584.
- (114) El-Sibert, I.; Reinhardt, W.; Hynes, J. Intramolecular Vibrational Relaxation and Spectra of CH and CD Overtones in Benzene and Perdeuterobenzene. *J. Chem. Phys.* **1984**, *82*, 1115–1134.
- (115) Press, W. H.; Teukolsky, S. A.; Vetterling, W. T.; Flannery, B. P. *Numerical Recipes in C*; Cambridge University Press: New York, 1992.
- (116) Golub, G. H.; Loan, C. F. V. *Matrix Computations*; The Johns Hopkins University Press: Baltimore, MD, 1996.
- (117) Romo, T. D.; Clarage, J. B.; Sorensen, D. C.; Phillips, G. N., Jr. Automatic Identification of Discrete Substates in Proteins: Singular Value Decomposition Analysis of Time-Averaged Crystallographic Refinements. *Proteins* **1995**, *22*, 311–321.
- (118) Mayo, S. L.; Olafson, B. D.; Goddard, W. A. DREIDING: A Generic Force Field for Molecular Simulations. *J. Phys. Chem.* **1990**, *94*, 8897.
- (119) Li, Y.; Zhu, F.; Vaidehi, N.; Goddard, W. A. Prediction of the 3D Structure and Dynamics of Human DP G-Protein Coupled Receptor Bound to an Agonist and Antagonist. *J. Am. Chem. Soc.* **2007**, *129*, 10720.
- (120) Iyengar, S. S.; Schlegel, H. B.; Millam, J. M.; Voth, G. A.; Scuseria, G. E.; Frisch, M. J. Ab Initio Molecular Dynamics: Propagating the Density Matrix with Gaussian orbitals. II. Generalizations Based on Mass-weighting, Idempotency, Energy Conservation and Choice of Initial Conditions. *J. Chem. Phys.* **2001**, *115*, 10291–10302.
- (121) Welch, B. L. The Generalization of "Student's" Problem When Several Different Population Variances are Involved. *Biometrika* **1947**, *34*, 28–35.
- (122) Sawilowsky, S. S. Fermat, Schubert, Einstein and Behrens-Fisher: The Probable Difference Between Two Means When  $\sigma_1 \neq \sigma_2$ . *JMASM* **2002**, *1*, 461–472.
- (123) Haile, S. M.; Boysen, D. A.; Chisholm, C. R. I.; Merle, R. B. Solid Acids as Fuel Cell Electrolytes. *Nature* **2001**, *410*, 910.
- (124) Hudson, B. S.; Verdal, N. Vibrational Dynamics in Short, Strong Symmetric Hydrogen Bonds: General Considerations and Two Examples. *Phys. B: Condensed Matter* **2006**, *385*, 212–215.
- (125) Gertner, B. J.; Hynes, J. T. Molecular Dynamics Simulation of Hydrochloric Acid Ionization at the Surface of Stratospheric Ice. *Science* **1996**, *271*, 1563–1566.
- (126) Devlin, J. P.; Uras, N.; Sadlej, J.; Buch, V. Discrete Stages in the Solvation and Ionization of Hydrogen Chloride Adsorbed on Ice Particles. *Nature* **2002**, *417*, 269–271.
- (127) Aloisio, S.; Francisco, J. S. Radical Water Complexes in Earth's Atmosphere. *Acc. Chem. Res.* **2000**, *33*, 825–830.
- (128) Roscioli, J. R.; McCunn, L. R.; Johnson, M. A. Quantum Structure of the Intermolecular Proton Bond. *Science* **2007**, *316* (5822), 249–254.

- (129) Petersen, M.; Iyengar, S. S.; Day, T.; Voth, G. A. The Hydrated Proton at the Water Liquid/Vapor Interface. *J. Phys. Chem. B* **2004**, *108* (39), 14804–14806.
- (130) Iyengar, S. S.; Day, T. J. F.; Voth, G. A. On the Amphiphilic Behavior of the Hydrated Proton: An Ab Initio Molecular Dynamics Study. *Int. J. Mass Spectrom.* **2005**, *241*, 197–204.
- (131) Schlegel, H. B.; Millam, J. M.; Iyengar, S. S.; Voth, G. A.; Daniels, A. D.; Scuseria, G. E.; Frisch, M. J. Ab Initio Molecular Dynamics: Propagating the Density Matrix with Gaussian Orbitals. *J. Chem. Phys.* **2001**, *114*, 9758–9763.
- (132) Schlegel, H. B.; Iyengar, S. S.; Li, X.; Millam, J. M.; Voth, G. A.; Scuseria, G. E.; Frisch, M. J. Ab Initio Molecular Dynamics: Propagating the Density Matrix with Gaussian orbitals. III. Comparison with Born-Oppenheimer Dynamics. *J. Chem. Phys.* **2002**, *117*, 8694–8704.
- (133) Iyengar, S. S.; Schlegel, H. B.; Voth, G. A.; Millam, J. M.; Scuseria, G. E.; Frisch, M. J. Ab Initio Molecular Dynamics: Propagating the Density Matrix with Gaussian orbitals. IV. Formal Analysis of the Deviations from Born-Oppenheimer Dynamics. *Isr. J. Chem.* **2002**, *42*, 191–202.
- (134) Iyengar, S. S.; Frisch, M. J. Effect of Time-Dependent Basis Functions and Their Superposition Error on Atom-Centered Density Matrix Propagation (ADMP): Connections to Wavelet Theory of Multi-Resolution Analysis. *J. Chem. Phys.* **2004**, *121*, 5061–5070.
- (135) Iyengar, S. S.; Schlegel, H. B.; Voth, G. A. Atom-Centered Density Matrix Propagation: Generalizations Using Bohmian Mechanics. *J. Phys. Chem. A* **2003**, *107*, 7269–7277.
- (136) Iyengar, S. S.; Petersen, M. K.; Day, T. J. F.; Burnham, C. J.; Teige, V. E.; Voth, G. A. The Properties of Ion-Water Clusters. I. The Protonated 21-Water Cluster. *J. Chem. Phys.* **2005**, *123*, 084309.
- (137) Iyengar, S. S. Further Analysis of the Dynamically Averaged Vibrational Spectrum for the “Magic” Protonated 21-Water Cluster. *J. Chem. Phys.* **2007**, *126*, 216101.
- (138) Iyengar, S. S. Dynamical Effects on Vibrational and Electronic Spectra of HO<sub>2</sub> Water Cluster: An Ab Initio Molecular Dynamics Study. *J. Chem. Phys.* **2005**, *123*, 084310.
- (139) Li, X.; Teige, V. E.; Iyengar, S. S. Can the Four-Coordinated, Penta-Valent Oxygen in Hydroxide Water Clusters Be Detected Through Experimental Vibrational Spectroscopy? *J. Phys. Chem. A* **2007**, *111*, 4815–4820.
- (140) Pacheco, A. B.; Dietrick, S. M.; Stevens, P. S.; Iyengar, S. S. Pump-Probe” Atom-Centered Density Matrix Propagation Studies to Gauge Anharmonicity and Energy Repartitioning in Atmospheric Reactive Adducts: Case Study of the OH + Isoprene and OH + Butadiene Reaction Intermediates. *J. Phys. Chem. A* **2012**, *116*, 4108.
- (141) Dietrick, S. M.; Pacheco, A. B.; Phatak, P.; Stevens, P. S.; Iyengar, S. S. The Influence of Water on Anharmonicity, Stability and Vibrational Energy Distribution of Hydrogen-Bonded Adducts in Atmospheric Reactions: Case Study of the OH + Isoprene Reaction Intermediate Using Ab-Initio Molecular Dynamics. *J. Phys. Chem. A* **2012**, *116*, 399–414.
- (142) Bakowies, D.; Thiel, W. Hybrid Models for Combined Quantum Mechanical and Molecular Mechanical Approaches. *J. Phys. Chem.* **1996**, *100*, 10580.
- (143) Swope, W. C.; Andersen, H. C.; Berens, P. H.; Wilson, K. R. A Computer-Simulation Method for the Calculation of Equilibrium Constants for the Formation of Physical Clusters of Molecules: Application to Small Water Clusters. *J. Chem. Phys.* **1982**, *76*, 637–649.